

AD-A245 813

DOCUMENTATION PAGE

Form Approved
OMB No. 0704-0188

2b DECLASSIFICATION/DOWNGRADING SCHEDULE <u>Unclassified</u>		1b RESTRICTIVE MARKINGS	
4 PERFORMING ORGANIZATION REPORT NUMBER(S) N00014-89-J-1237		3 DISTRIBUTION/AVAILABILITY OF REPORT Approved for public release; distribution unlimited.	
6a NAME OF PERFORMING ORGANIZATION Colorado State University	6b OFFICE SYMBOL (if applicable)	5 MONITORING ORGANIZATION REPORT NUMBER(S)	
6c ADDRESS (City, State, and ZIP Code) Department of Chemistry Fort Collins, CO 80523		7a NAME OF MONITORING ORGANIZATION	
8a NAME OF FUNDING/SPONSORING ORGANIZATION Office of Naval Research		7b ADDRESS (City, State, and ZIP Code)	
8b OFFICE SYMBOL (if applicable)		9 PROCUREMENT INSTRUMENT IDENTIFICATION NUMBER N00014-89-J-1237	
8c ADDRESS (City, State, and ZIP Code) 800 North Quincy Street Arlington, VA 22217-5000		10 SOURCE OF FUNDING NUMBERS	
		PROGRAM ELEMENT NO	PROJECT NO
		TASK NO	WORK UNIT ACCESSION NO
11 TITLE (Include Security Classification) <u>Toluene-Water Clusters: Ion Fragmentation and Chemistry (Unclassified)</u>			
12 PERSONAL AUTHOR(S) <u>Shijian Li and Elliot R. Bernstein</u>			
13a TYPE OF REPORT Technical Report	13b TIME COVERED FROM _____ TO _____	14 DATE OF REPORT (Year, Month, Day) February 4, 1992	15 PAGE COUNT
16 SUPPLEMENTARY NOTATION <u>toluene water cluster ion fragmentation, one and two-color mass resolved excitation spectroscopy, nanosecond time scale, nozzle-laser delay timing, time resolved pump</u>			
17 COSATI CODES		18 SUBJECT TERMS (Continue on reverse if necessary and identify by block number)	
FIELD	GROUP	SUB-GROUP	
19 ABSTRACT (Continue on reverse if necessary and identify by block number) SEE ATTACHED ABSTRACT			
20 DISTRIBUTION/AVAILABILITY OF ABSTRACT <input checked="" type="checkbox"/> UNCLASSIFIED/UNLIMITED <input type="checkbox"/> SAME AS RPT <input type="checkbox"/> DTIC USERS		21 ABSTRACT SECURITY CLASSIFICATION Unclassified	
22a NAME OF RESPONSIBLE INDIVIDUAL Elliot R. Bernstein		22b TELEPHONE (Include Area Code) (303) 491-6347	22c OFFICE SYMBOL

DTIC
ELECTE
S B D
FEB 12 1992

OFFICE OF NAVAL RESEARCH

Contract N00014-89-J-1237

TECHNICAL REPORT #76

Toluene-Water Clusters: Ion Fragmentation and Chemistry

by

E. R. Bernstein, S. Li

Submitted to

Journal of Chemical Physics


Department of Chemistry
Colorado State University
Fort Collins, Colorado 80523

February 4, 1992

Reproduction in whole or in part is permitted for
any purpose of the United States Government.

This document has been approved for public release
and sale; its distribution is unlimited

92 2 10 10 3

92-03349


ABSTRACT

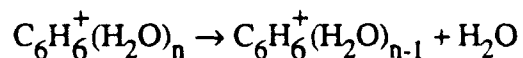
Toluene/water cluster ion fragmentation is studied for isolated cold clusters by means of one- and two-color mass resolved excitation spectroscopy, time resolved pump ($S_1 \leftarrow S_0$) probe ($I \leftarrow S_1$) spectroscopy on the nanosecond time scale, and nozzle-laser delay timing experiments. These experiments lead to an identification of parent clusters for all fragment ion clusters observed. Fragmentation reactions depend on cluster size and on the energy deposited in the ion by the two photon $I \leftarrow S_1 \leftarrow S_0$ excitation sequence. Fragments identified by these techniques include $(H_2O)_x H^+$ ($x = 3, 4$) and $\text{toluene}^+(H_2O)_{n-1}$ for $\text{toluene}(H_2O)_n$ clusters and $(H_2O)_x D^+$, $(H_2O)_x H^+$ and $\text{toluene-d}_3^+(H_2O)_{n-1}$ for $\text{toluene-d}_3(H_2O)_n$ clusters. For $n \leq 3$ the preferred cluster fragmentation pathway is loss of a single H_2O molecule, while for $n \geq 4$ the preferred cluster fragmentation pathway is generation of $(H_2O)_n H^+$. Cluster ion fragmentation is prevalent in this system because of product stability (i.e., solvated protons and the benzyl radical) and because the $I \leftarrow S_1$ transition leaves the cluster ion in a very highly excited vibrational state ($\Delta v \gg 0$ for the $I \leftarrow S_1$ transition). The fragmentation of $\text{toluene}^+(H_2O)_3$ to generate $(H_2O)_3 H^+$ and a benzyl radical takes place by two distinct pathways with generation times $\tau_1 < 60$ ns and $\tau_2 = 480$ ns. The $\text{toluene}^+(H_2O)_2$ fragment from $\text{toluene}^+(H_2O)_3$ has a generation time of $\tau < 60$ ns. The possible energetics, kinetics and mechanisms for these fragmentations are discussed.

Accession For	
NTIS GRA&I	<input checked="" type="checkbox"/>
DTIC TAB	<input type="checkbox"/>
Unannounced	<input type="checkbox"/>
Justification	
By	
Distribution/	
Availability Codes	
Dist	Avail and/or Special
A-1	

I. INTRODUCTION

The study of clusters composed of an aromatic molecule (solute) and a number of small molecules (solvent species) is motivated by three main concerns: 1. solvation effects on isolated molecule structure and energy levels;¹ 2. energy dynamics in condensed phases (under solvation conditions) compared to energy dynamics in isolated molecules;² and 3. the effect of solvation on unimolecular and bimolecular chemistry.³ Observed cluster behavior is, in general, different for polar and non-polar solvents. The behavior of clusters consisting of a solute molecule and non-polar solvents is characterized typically by small shifts from isolated molecule spectra, sharp (molecular-like) ionization thresholds, no cluster fragmentation at the (apparent) ionization threshold, simple vibrational dynamics (intracuster vibrational distribution-IVR) and unimolecular vibrational predissociation (VP) reactions, and no evident intermolecular chemistry in any accessed electronic state (i.e., ground state, first excited singlet state, and the cluster ion ground electronic state). The behavior of clusters consisting of a solute molecule and polar solvents (e.g., NH₃, H₂O, ROH, NR₃, etc.) is quite different: broad ionization thresholds,⁴ extensive cluster fragmentation at the apparent ionization threshold,⁵ and cluster S₁ and/or ion chemistry⁶ (*vide infra*) are all quite typical.

In the extreme case, recently reported for benzene/water clusters,⁷ the ion fragmentation reaction



apparently cannot be avoided. Other more extreme examples of cluster ion chemistry can be found in the toluene/water and ammonia systems for which both the above fragmentation reaction and reactions generating (H₂O)_nH⁺ (n ≥ 3), and (NH₃)_mH⁺ (m ≥ 1, n > m) can be characterized.⁸ (Throughout this paper we use the letter n to signify the number of solvent molecules in the original parent cluster prior to fragmentation of the ion.)

In this report we explore the cluster ion chemistry of toluene/water clusters. The chemistry of toluene/ammonia cluster ions is dealt with in a separate report. The particular focus of this paper concerns four main themes: association of a given resolved spectrum with a specific cluster $C_6H_5CH_3(H_2O)_n$; identification of particular cluster ion fragmentation patterns as a function of ionization energy; demonstration that the observed chemistry does indeed occur on the ground state ion potential surface and not the S_0 , S_1 or T_n surfaces; and association of (qualitative) cluster structure with the observed chemistry.

II. EXPERIMENTAL PROCEDURES

The reported experimental results are mass resolved excitation spectra (MRES).⁹ Both one- and two-color experiments are carried out. For one-color experiments, a single Nd/YAG pumped dye laser is employed to excite the cluster or molecule to S_1 and subsequently to ionize it, generating both the $S_1 \leftarrow S_0$ spectrum as the laser is scanned and the various ion signals. The dye used in these experiments is LDS698: the fundamental output of the dye laser is doubled and mixed with the 1064 nm fundamental output of the Nd/YAG pump laser. Other experimental conditions include: helium backing pressure at 50 psi and toluene and water saturated vapor pressure maintained at $T \sim 300$ K. For two-color experiments, two separate Nd/YAG pumped dye lasers are employed, one of which induces the $S_1 \leftarrow S_0$ transition and the other induces the $I \leftarrow S_1$ transition. Both lasers can be scanned to generate "spectra" of the two different transitions. The ionization dye laser for these two-color experiments uses DCM, R640 or kiton red as the lasing medium. Scanning the ionization dye laser for a fixed excitation energy yields ionization threshold spectra. Observing the ion signal intensity as a function of time separation between the two lasers in a two-color ionization experiment yields the lifetimes of various ion signals originating from the S_1 state.

Information about cluster size can additionally be obtained by noting the time delay between nozzle opening and the initial appearance of signal intensity in a given mass

channel. Signals which arise from cluster fragmentation will still have a nozzle/signal time delay indicative of the parent cluster. This time delay is associated with two phenomena: 1. flow speed differences (velocity slippage) in the supersonic expansion for different masses; and 2. cluster formation within the nozzle opening time. The heavier the cluster mass the larger is the time delay between nozzle opening and maximum signal observation as velocity slippage is greater for larger masses and larger clusters are formed later in the nozzle opening sequence. While neither of these factors can be effectively predicted a priori, the time differences can be utilized to distinguish parent clusters from fragment clusters. In order to acquire such data the time delay between nozzle opening and laser firing is scanned for given transitions in different mass channels and plotted on a single graph. Signals arising in different mass channels but associated with a given parent cluster will all have the same time delay with regard to nozzle and laser firing, even though their flight times in the drift tube between the ion acceleration region and the mass detector are quite different.

III. EXPERIMENTAL RESULTS

A. One-Color Mass Resolved Excitation Spectra

One-color MRES observed in mass channels appropriate for toluene(H_2O)_m ($m = 1, \dots, 4$) clusters are presented in Figures 1a through 1d. The negative features in these spectra are caused by microchannel plate overload at the toluene flight time. Two vibrational progressions can be identified in the toluene (H_2O)₁ mass channel (Figure 1a): one of 7 cm^{-1} spacing and the other of 50 cm^{-1} spacing. Transitions labeled **p** and **q** in Figure 1a are vibrational features of the toluene/water clusters (n , the number of solvent molecules in the parent cluster, is not yet clear) which appear at 37579 and 37531 cm^{-1} , respectively. To reveal the nature of these vibrational motions, isotopic substitution of both the toluene methyl group and the water molecules can be pursued. Deuteration of the

toluene (free) methyl rotor yields no shifts of any observed cluster transitions near the 0_0^0 structure of toluene(H_2O) $_m$ ($m = 1, \dots, 4$) clusters. Deuteration of the water to form toluene(D_2O) $_n$ clusters yields a 6% ($\sim 0.5 \text{ cm}^{-1}$) red shift in the 7 cm^{-1} motion and less than 1% ($\sim 0.5 \text{ cm}^{-1}$) blue shift in the 50 cm^{-1} progression observed in the toluene(H_2O) $_1$ mass channel. Given these results one can tentatively conclude that the observed features in the toluene(H_2O) $_1$ mass channel are not due to methyl rotor transitions or a given water molecule rotation about its own symmetry (C_2) axis. These data (Figure 1a) suggest that the generator of the spectrum observed in the toluene(H_2O) $_1$ mass channel may not be associated with the toluene(H_2O) $_1$ cluster. The pattern of this spectrum also suggests a difference of parent cluster geometry in the S_0 and S_1 electronic states.

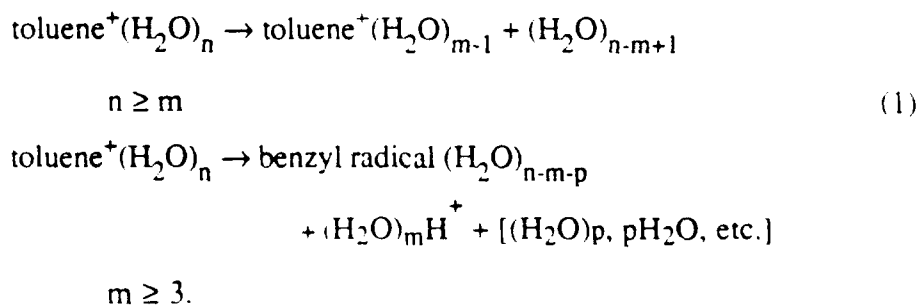
Figures 1b and 1c show one-color MRES observed in the toluene(H_2O) $_2$ and toluene(H_2O) $_3$ mass channels. Peaks labeled **a** and **b** are found at 37606 and 37591 cm^{-1} , respectively. Features **a** and **b** are followed by weak features at ca. 14 cm^{-1} to higher energy. Feature **b** is not found in mass channels toluene (H_2O) $_{2,4}$; however, the first small feature following peak **b** in the toluene(H_2O) $_3$ mass channel coincides with peak **a** in the toluene(H_2O) $_{1,2}$ channel. Apparently this feature (**a**) is common to all three mass channels, toluene(H_2O) $_{1,2,3}$; this suggests, in general, that feature **a** in the toluene(H_2O) $_{1,2}$ mass channels may well be a fragment feature associated with toluene(H_2O) $_n$, $n \geq 3$.

Three intense features (**c,d,e**, Figure 1d) can be identified in the toluene(H_2O) $_4$ mass channel. Features **d** and **c** also appear in the toluene(H_2O) $_3$ mass channel. The different behavior found for these three features suggests that feature **e** is of different parentage than features **d** and **c**.

One-color MRES also appear for toluene(H_2O) $_n$ clusters in mass channels 55 [$(\text{H}_2\text{O})_3\text{H}^+$], 73 [$(\text{H}_2\text{O})_4\text{H}^+$], 91 [$(\text{H}_2\text{O})_5\text{H}^+$] and 109 [$(\text{H}_2\text{O})_6\text{H}^+$] amu as shown in Figures 2a through 2d. The main features in these spectra are labeled according to the feature designations given in Figure 1. Signals in mass channel 127 [$(\text{H}_2\text{O})_7\text{H}^+$] are too

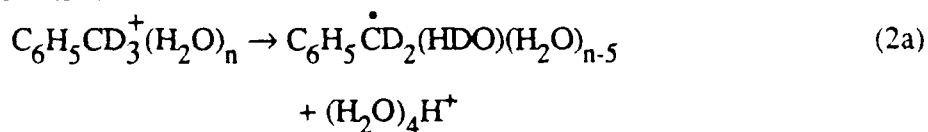
weak to record reliably. One-color MRES for toluene-d₃(H₂O)_n clusters are also observed in fragment mass channels 56 [(H₂O)₄D⁺], 73 [(H₂O)₄H⁺] and 74 [(H₂O)₄D⁺] as presented in Figures 3a to c. Again, all transitions are labeled according to the notation of Figure 1. Transitions for toluene(H₂O)_n clusters are labeled by unprimed letters (a, b, c, d, e) and transitions for toluene-d₃(H₂O)_n clusters are labeled with primed letters (a', b', c', d', e'). The MRES spectra presented in Figures 2a (55 amu) and 3a (56 amu) and 2b (73 amu) and 3c (74 amu) are identical except for isotopic shift. One H or D ion must be transferred from the toluene CD₃ or CH₃ methyl group to the (H₂O)_n (n ≥ 3). The remaining fragments in this reaction must be water molecules and the (perhaps solvated) benzyl radical. The signals observed in mass channel 91 (Figure 2c) are due to both (H₂O)₅H⁺ and the benzyl radical ion. Of course, in both instances, the one-color MRES observed is associated with either toluene or the appropriate parent cluster. Features in Figure 2c observed due to the benzyl radical as generated by bare molecule toluene fragmentation are found at 37482 cm⁻¹ (toluene 0₀⁰), 37,498, 37,536 and 37,560 cm⁻¹ (toluene methyl rotor transitions), and 37648 cm⁻¹ (toluene vibration). The methyl rotor feature at 37,536 cm⁻¹ is label T₃. The transitions c, d, e, observed in the 91 amu mass channel ((H₂O)₅H⁺) are the same as observed in the toluene(H₂O)₄ mass channel in one-color MRES and thus arise from toluene(H₂O)_n n≥5 clusters.

The pattern of these results is quite regular: features that appear in the toluene(H₂O)_{m-1} mass channel also appear in the (H₂O)_mH⁺ mass channel for m = 3, 4, 5. The following fragment reactions (although not exclusively) are suggested by the data presented in Figures 1, 2, 3:

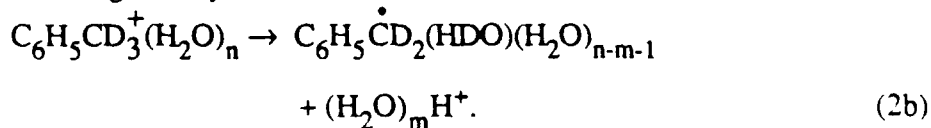


Under the likely assumption that $p = 0$, peak **e** is associated with toluene(H_2O)₆, peaks **d**, **c** are associated with toluene(H_2O)₅, peak **b** is associated with toluene(H_2O)₄ and peak **a** is associated with toluene(H_2O)₃. No reproducible features can be found for either the (H_2O) H^+ or (H_2O)₂ H^+ mass channels suggesting that at least three water molecules are required to solvate a proton before this reaction becomes thermodynamically favorable or before the reaction (kinetic) barrier for this channel can be significantly reduced. The deuterated toluene rotor studies make clear that the proton in the (H_2O)_n H^+ cluster comes from the methyl group of toluene.

One-color MRES signals for toluene- d_3 (H_2O)_n can also be found in the (H_2O)₄ H^+ (73 amu, Figure 3b) mass channel. These features are about 10 times weaker than those of (H_2O)₄ D^+ (74 amu, Figure 3c). Features **b**, **c**, **d** in Figure 3b are due to residual toluene- h_3 in the nozzle which has formed clusters with water molecules (compare to Figure 2b). Features **d'** and **c'** (isotopically shifted **d** and **c**) are known to be associated with higher order clusters as shown in Figure 2c. Thus one can conclude, based on these figures, that the reaction



has taken place. More generally one can write



The fact that a **b'** transition is not found in the spectrum presented in Figure 3b but is found in Figure 3c suggests that H/D exchange as given above is not possible for this transition. This in turn indicates either that the **b/b'** transition arises from the toluene(H_2O)₄ parent cluster, or that the geometry of this cluster is such that H/D exchange is prohibited.

A general observation about all these fragmentation reaction paths can be made based on the relative intensities of common signals in the different mass channels.

Signals observed in the $(\text{H}_2\text{O})_3\text{H}^+$ mass channel are several times weaker than the same signals in the toluene $(\text{H}_2\text{O})_2$ mass channel. On the other hand, signals observed in the $(\text{H}_2\text{O})_5\text{H}^+$ mass channel are several times stronger than those same signals observed in the toluene $(\text{H}_2\text{O})_4$ mass channel. Thus, fragmentation to toluene $(\text{H}_2\text{O})_2$ is more favorable than fragmentation to the benzyl radical and $(\text{H}_2\text{O})_3\text{H}^+$, but the reaction thermodynamics and/or kinetics change for toluene $(\text{H}_2\text{O})_n$, $n \geq 5$. These intensity ratios probably obtain because the proton is better solvated in a $(\text{H}_2\text{O})_5$ cluster than a $(\text{H}_2\text{O})_3$ cluster.

Absence of signals for any feature in the $(\text{H}_2\text{O})_2\text{H}^+$ and $(\text{H}_2\text{O})_1\text{H}^+$ mass channels indicates that cluster fragmentation into these channels is not favorable, most likely due to the relatively low gas phase basicity of $(\text{H}_2\text{O})_{1,2}$: note, however, that the same reaction for toluene/ammonia does generate $(\text{NH}_3)_m\text{H}^+$, $m = 1, 2, 3, \dots$ ⁸

On the basis of the one-color mass resolved excitation thus far presented, multiple cluster conformers for a given cluster mass (size) do not seem to be present.

B. Two-Color Mass Resolved Excitation Spectroscopy

The two-color MRES observed in toluene $(\text{H}_2\text{O})_n$, $n = 1, \dots, 5$ mass channels are presented in Figure 4. Intense features marked with lower case letters correspond to similarly marked features in Figures 1 through 3. All one-color toluene $(\text{H}_2\text{O})_{n-1}$ features now clearly appear in the toluene $(\text{H}_2\text{O})_n$ mass channel. Note, in particular, that transition **a** does not appear in the toluene $(\text{H}_2\text{O})_4$ mass channel, and that transition **b** does not appear in the toluene $(\text{H}_2\text{O})_5$ mass channel. Thereby, we suggest that feature **a** is due to toluene $(\text{H}_2\text{O})_3$, feature **b** is due to toluene $(\text{H}_2\text{O})_4$ and feature **c** and **d** are due to toluene $(\text{H}_2\text{O})_5$, etc. Additionally, four new features appear (uniquely) in the toluene $(\text{H}_2\text{O})_1$ mass channel (indicated by arrows in Figure 4a). We suggest that these four new features actually arise from toluene $(\text{H}_2\text{O})_1$ clusters and that most of the spectra recorded by one-color MRES for this mass channel are due to toluene $(\text{H}_2\text{O})_2$. These conclusions are summarized in Table I and Scheme I.

To get a clearer picture of the spectrum of the toluene(H_2O)₁ cluster, a difference spectrum between toluene(H_2O)₁ (Figure 4a) and (H_2O)₂ (Figure 4b) is calculated and presented in Figure 5a. Transitions marked by the letter O_i ($i = 1, \dots, 4$) are due to toluene(H_2O)₁. Toluene signals appearing in other mass channels are generated by varying degrees of detector overload from the very intense toluene features. The negative peak at 37606 cm^{-1} is due to feature **a** (parent toluene(H_2O)₃). The toluene(H_2O)₁ features can also be observed in the toluene mass channel (Figure 5b) due to toluene(H_2O)₁ fragmentation.

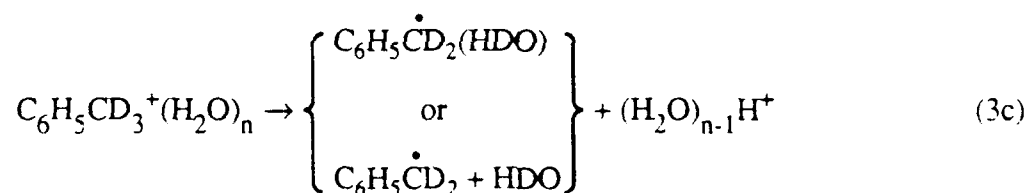
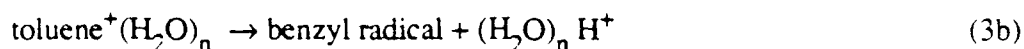
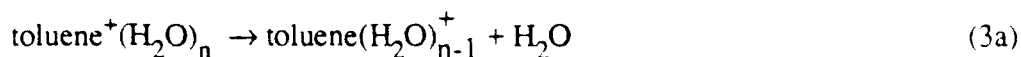
All observed signals are due to absorption of two and only two photons. This is well illustrated in Figure 6 in which the transition **b** (see Figures 1-4) is excited (37591 cm^{-1}) for both one- and two-color mass resolved excitation spectra. The ionization laser is at an energy of 34350 cm^{-1} for two-color spectra. If the ionization laser is increased in intensity, new features in different mass channels (e.g., 63, 65, 75, 77, 102 amu) can be observed (Figure 6b). Reducing the laser power only slightly returns the mass spectrum to its original low power ionization status (Figure 6c).

C. Time Delay Studies

In Figure 7 we present various toluene(H_2O)_n $n = 0, \dots, 6$ signal intensities (labeled as in Figures 1-4 and Table I) as a function of time delay between nozzle triggering and laser excitation. These data show quite dramatically the following points: 1. the time separation between T_3 and **q** represents a "double" separation - feature **q** is due to toluene(H_2O)₂ and T_3 is due to toluene; 2. features **p** and **q** are generated by a cluster of the same mass, toluene(H_2O)₂; 3. heavier mass clusters are formed more closely together in the expansion and suffer flight time and/or condensation compression as can be seen from the time delay behavior of features **q**, **a**, **b**, **c**. These data are in agreement with the conclusions reached above from both one- and two-color MRES: 1. feature **e** is generated by parent toluene(H_2O)₆ or (H_2O)₇; 2. features **c** and **d** are generated by parent toluene(H_2O)₅; 3. feature **b** is generated by toluene(H_2O)₄; 4. feature **a** is generated by

toluene(H_2O)₃; 5. features **p** and **q** are generated by toluene(H_2O)₂; and 6. the missing toluene(H_2O)₁ cluster spectra are located by two-color MRES techniques and are presented in Figure 5 as **O_i**. These conclusions are summarized in Table I and Scheme I.

Some additional general comments can now be made regarding the fragmentation processes observed: 1. the typical fragmentation reactions presented in eq. (1) hold mainly with $m = n$ and $p = 0$; 2. the benzyl radical is generated usually without solvation; and 3. toluene/water cluster geometry is such that H/D exchange (as depicted in eq. (2)) can occur for the larger toluene- d_3 /water clusters. These results are summarized in the following equations:

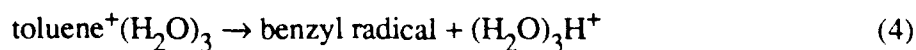


Two-color MRES studies as a function of time delay between the two lasers have been performed for all the labeled transitions **a**, **b**, **c**, **d**, **e**. For example, transition **a** signals observed in all three mass channels, (H_2O)₃H, toluene(H_2O)₂, and toluene(H_2O)₃, have identical lifetimes of about 65 ns: this is the same lifetime as the toluene S_1 state. We thus conclude that the observed chemistry and energy dynamics of the toluene/water system are not related in any way to the toluene triplet manifold or the ground state: all the competitive fragmentation reactions that are observed for the toluene/water system must take place in the ground electronic state of the ion. Recall that all presented excitations $S_1 \leftarrow S_0$ take place with no vibrational excess energy generated in the cluster.

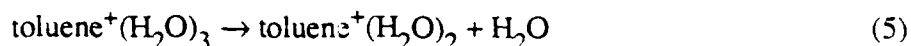
The third time dependent measurement needed to help elucidate the mechanisms and kinetics of the observed dissociation and proton transfer/fragmentation reactions is a study of the signal intensity as a function of flight time: in particular we are concerned about signal "line shape" for given mass channel features. These one-color and two-color MRES results are displayed in Figure 8. The transitions presented are feature **a** detected in the $(\text{H}_2\text{O})_3\text{H}$ mass channel, feature **T₃** detected in the toluene mass channel, and feature **a** detected in both the toluene $(\text{H}_2\text{O})_2$ fragment and toluene $(\text{H}_2\text{O})_3$ parent mass channels (see Figures 1-4 and Table I). Transition **a** in the $(\text{H}_2\text{O})_3\text{H}$ mass channel (Figure 8a) rises in mass channel 55 amu, but spreads (decays) to "higher mass channels" or longer flight times. In the two-color experiment the ionization laser energy is varied between 34,900 and 37,600 cm^{-1} with no effect on the observed signal time width. On the other hand, transition **a** detected in the toluene $(\text{H}_2\text{O})_2$ mass channel does not show this "decay behavior" (Figure 8c). Moreover, neither do any of the other signals (Figure 8b, d).

We note the following additional information concerning these observations: 1. exactly the same behavior is found for transition **a'** of the toluene- $\text{d}_3(\text{H}_2\text{O})_3$ as detected in the $(\text{H}_2\text{O})_3\text{D}$ (56 amu) mass channel; 2. the width of the mass channel 55 and 56 amu features is due to a single mass peak and a single, resolved spectroscopic feature (**a** and **a'** in this instance); 3. various positions in the width of roughly eight to ten mass channels yield the same optical spectrum (feature **a** or **a'**); 4. the apparent sharp features to higher mass in the two-color signal at mass channel 55 amu are due to fragmentation associated with the high intensity of the ionization laser needed to generate the strong feature displayed; and 5. both the one-color and two-color MRES signals in mass channel 55 and 56 amu give the same decay constants.

These observations suggest that the reaction



takes place slowly (ca. 500 ns). Upon careful analysis of the line shape of the 55 amu $(\text{H}_2\text{O})_3\text{H}^+$ time of flight signal, this feature can be resolved into a <60 ns and a 480 ns generation time, as will be shown below. On the other hand, the reaction



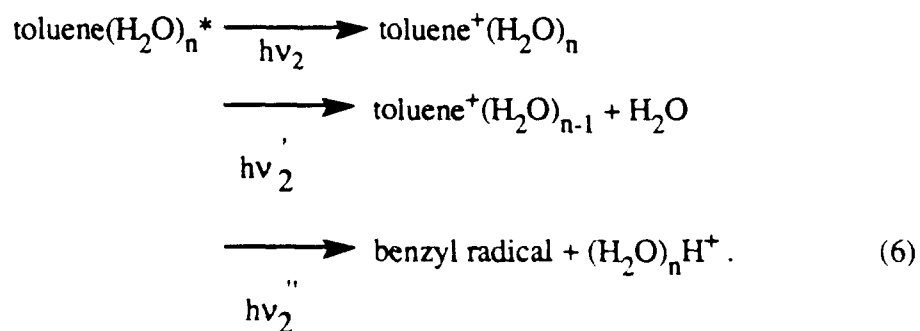
can be deconvolved into only a ca. <60 ns generation time (the instrument response function in roughly 20 ns fwhm) after the parent cluster has been ionized. These data suggest the following physical behavior for the fragmentation of the toluene $(\text{H}_2\text{O})_3$ cluster:

1. two pathways exist to generate the $(\text{H}_2\text{O})_3\text{H}^+$ fragment, one fast <60 ns and one slow ca. 480 ns; and
2. a single pathway exists to generate the $\text{toluene}^+(\text{H}_2\text{O})_2$ fragment.

Contributions from fragmentation kinetic energy render a better estimate of the fast generation time difficult to make. A detailed discussion of the analysis of these MRES line shapes is presented in the Discussion Section. In the Discussion Section we will present a mechanism for the above reactions designed to rationalize these observations.

D. Apparent Threshold Ionization Energies

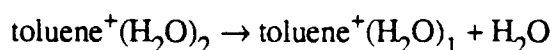
Ionization action spectra are recorded for each cluster as detected through the parent and fragment mass channel signals. Thus, an appearance or apparent ionization energy can be found for each reaction:



A few examples of such spectra are presented in Figure 9. Figure 9a shows the ionization action spectrum of transition T_3 of bare toluene. The toluene transitions have a sharp ionization threshold with a $\Delta v = 0$ Franck-Condon factor maximum. Clusters with nonpolar solvents typically have similar ionization threshold behavior as shown for

benzene(CH₄)₁ in Figure 9b. On the other hand, toluene(H₂O)₂ has a gradually increasing threshold over several thousands of cm⁻¹. Figure 9c shows the first ~ 500 cm⁻¹ of this low rise for the transition labeled **q** in Figures 1-4 and Table I. For this latter cluster the Franck-Condon factor must favor large Δv and therefore the two accessed potential surfaces S_1 and I must be displaced from one another and of a different shape. The behavior displayed for toluene(H₂O)₂ transition **q** in Figure 9c is typical of all toluene/water cluster transitions. The S_1 and I states must have significantly different geometries for the toluene/water cluster system.

Threshold ionization data for the various parent clusters detected in the toluene(H₂O)_n, toluene(H₂O)_{n-1}, and (H₂O)_nH mass channels are presented in Table II. Note that the ionization threshold for toluene is about 2000 cm⁻¹ higher than that for toluene(H₂O)₄. The appearance threshold for the reaction

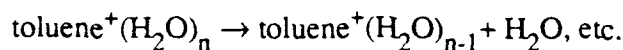


is about 1000 cm⁻¹ above the toluene(H₂O)₂ ionization threshold. The toluene(H₂O)₄ cluster will generate three different products depending on the ionization energy. For example, the toluene⁺(H₂O)₄ appears at a threshold energy of 68940 cm⁻¹. The toluene⁺(H₂O)₃ product requires 1300 cm⁻¹ more energy to appear and the (H₂O)₄H⁺ fragment requires 1100 cm⁻¹ more energy to appear. These data are summarized in Table II.

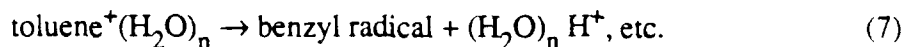
From the data presented in Table II one can extract the following generalizations concerning toluene/water ionization thresholds for reaction: 1. the ion state in the toluene/water cluster system is significantly stabilized with respect to the S_0 and S_1 cluster state and the bare toluene molecule, especially for large clusters; 2. the appearance potential for the (H₂O)_n H⁺ product is lower than that for the toluene⁺(H₂O)_{n-1} product for $n \geq 3$; and 3. fragmentation of higher order clusters (see eq. (3)) into the toluene(H₂O)_{1,2} channels takes more energy than fragmentation into the toluene(H₂O)₃ mass channel.

IV. DISCUSSION

Two different types of fragmentation are observed:



and



Cluster ion fragmentation to $(\text{H}_2\text{O})_{n-m}\text{H}^+$ is possible as long as $(n-m) \geq 3$. This behavior is probably related to the gas phase basicity of water because toluene/ammonia clusters can fragment to $(\text{NH}_3)_y\text{H}^+$, $y = 1, 2, 3, \dots$

These two paths are governed by intracuster vibration redistribution (IVR), vibrational predissociation (VP), proton transfer and overall reaction energy balance. The simple dissociation reactions must be governed by IVR and VP kinetics. The proton transfer/dissociation reaction is governed by the stability of the products which include the benzyl radical and the solvated proton. Evidently the proton affinities (properly, gas phase basicities) of H_2O and $(\text{H}_2\text{O})_2$ are not large enough to drive the reaction for H_3O^+ and $(\text{H}_2\text{O})_2\text{H}^+$. Since both the binding energies and the Franck-Condon shift for the $I \leftarrow S_1$ transition are unknowns, we cannot be more specific concerning the energy balance and dynamics of these two paths.

A. Cluster Structure

While only limited information concerning cluster geometry is available from the data presented in this report, some qualitative notions of cluster structure can be gained from these results.

First, we suggest that the water molecules in these clusters are themselves clustered into n -mers for the following reasons: spectroscopic shifts are all small and similar for the $S_1 \leftarrow S_0$ transition in the various toluene $(\text{H}_2\text{O})_n$ clusters; the parent clusters readily fragment into large $(\text{H}_2\text{O})_n\text{H}^+$ ($n = 3, 4, 5, 6$) clusters; and each toluene $(\text{H}_2\text{O})_n$ ($n = 2, 3, 4, 6 \dots$) cluster has a spectrum comprised typically of a single origin feature. The latter point suggests the water cluster forms in the presence of toluene and then interacts

with it, consistent with the relative size of the $(\text{H}_2\text{O})_n$ interaction energy (ca. $2000 \text{ cm}^{-1}/\text{H}_2\text{O}$) and the toluene/water interaction energy (ca. $700 \text{ cm}^{-1}/\text{H}_2\text{O}$).

Second, an inner ($n \leq 3$) and outer ($n > 3$) layer of water molecules seems to be consistent with the experimental results. The data that suggest this type of structure are the following: toluene $(\text{H}_2\text{O})_n$ ($n = 2, 3$ and 4) fragmentation appearance energy differs for the toluene $(\text{H}_2\text{O})_{n-1}$ cluster mass channel (see Table II); similarity between toluene $(\text{H}_2\text{O})_3$ and toluene $(\text{H}_2\text{O})_4$ spectra (features **a** and **b**, in Figures 1-4 and Table I) suggests the fourth H_2O does not interact strongly with toluene; cluster geometry seems to change significantly upon excitation for toluene $(\text{H}_2\text{O})_n$ ($n \leq 2$) but not larger ($n \geq 3$) clusters; cluster $S_1 \leftarrow S_0$ energy shifts are greatest for $n \leq 3$ but almost non-existent for $n \geq 4$; and higher order clusters (toluene $(\text{H}_2\text{O})_{3+m}$ for $m > 0$) fragment into the toluene $(\text{H}_2\text{O})_3$ mass channel but not into the toluene $(\text{H}_2\text{O})_{1,2}$ mass channels (consider the behavior of feature **a** vs. feature **b** - see Figures 1-4 and Table I).

Third, the water molecules probably hydrogen bond together in a chain or cyclic structure because of the limited number of cluster configurations for a given parent cluster $n = 1, \dots, 4$.

Empirical potential energy calculations can be employed to obtain additional insight into the details of cluster structure for small toluene/water clusters ($n = 1, 2$). All calculations for the S_0 state of toluene $(\text{H}_2\text{O})_1$ suggest that the hydrogen atoms of water point toward the aromatic ring, in a "weak hydrogen bonding" interaction geometry. The S_1 cluster structure should be fairly similar, even though the $n = 2$ toluene/water cluster does undergo some water displacement upon excitation. This would clearly not be the best structure for the toluene $(\text{H}_2\text{O})_n$ cluster ions because the positive ring would be best solvated by the negative end of the water dipole pointed toward it. We thus expect a large geometry change upon $I \leftarrow S_1$ excitation for these clusters: a rotation of the water molecule(s) in the toluene/water cluster such then the oxygen atom of water would be closest to the ring would be consistent with this picture.

B. Fragmentation Patterns and Mechanisms

Parent clusters, their transitions and fragmentation paths are presented in Table I. A general summary of the fragmentation patterns observed is presented in Scheme I. Note that for all toluene/water clusters, fragmentation is nearly complete: even near threshold ionization, ion fragmentation is a dominant factor in the cluster ion behavior and detection. Similar and even more extensive fragmentation is also found for the toluene/ammonia cluster system.

Such extensive fragmentation is not usual for van der Waals clusters. For example, even one-color MRES spectra of simple aromatics (e.g., benzene, toluene, azines, etc.) clustered with non-polar solvents^{1,10} (e.g., rare gases, but not He, $C_n H_{2n+2}$, CF_4 , CO_2 , CO, N_2) do not show extensive fragmentation reactions. One would initially suggest that, since the binding energies in S_0 , S_1 , and I for polar solvents should be much larger than those for non-polar solvents, cluster ion fragmentation should be even less of a problem for aromatic/polar solvent clusters than it is for aromatic/non-polar solvent clusters. Nonetheless, this is clearly not the case and we can present two related arguments to make the observed extensive cluster ion chemistry seem reasonable. First, the cluster ion is much more tightly bound than either the S_0 or S_1 van der Waals toluene(H_2O)_n cluster in its equilibrium configuration. Therefore, not only is the ion cluster potential well deeper, but its equilibrium minimum is also shifted to smaller separation between aromatic and solvent. Additionally, as pointed out above, the water molecule orientation for the closest waters to the toluene ring should have a different (probably inverted) equilibrium orientation in the ion than they do in the S_0 or S_1 states. This equilibrium position shift ensures (through the Franck-Condon factor for the transition $I \leftarrow S_1$) that the optically accessed ion is highly vibrationally excited and $\Delta v \gg 0$ for the $I \leftarrow S_1$ transition. The cluster ion then even at "threshold ionization" can have a great deal of excess vibrational energy. This too explains the very broad threshold for the ion excitation spectra: the slope in Figure 9c represents the vibrational overlap for the Franck-Condon transition $I \leftarrow S_1$.

This slope probably reflects the ion potential surface curve many thousands of wavenumbers above the ion zero point state. Second, if the polar solvent can accept a proton (e.g., $(\text{H}_2\text{O})_n\text{H}^+$, $n \geq 3$ and $(\text{NH}_3)_m\text{H}^+$, $m \geq 1$) and thereby generate a very stable radical (e.g., benzyl), the overall fragmentation reaction becomes much more energetically favorable.

C. Fragmentation Kinetics

One additional piece of information is available concerning the fragmentation reactions. For $\text{toluene}^+(\text{H}_2\text{O})_3$, the fragments $\text{toluene}^+(\text{H}_2\text{O})_{1,2}$ and $(\text{H}_2\text{O})_3\text{H}^+$ are observed. The dissociation reaction is relatively fast (<60 ns) and proton transfer fragmentation (i.e., $(\text{H}_2\text{O})_3\text{H}^+$ generation) has both slow ($\tau_2 \sim 500$ ns) and fast ($\tau_1 < 60$ ns) components (see Figure 8).

To obtain more information from the width of these observed fragment mass channel signals, we must relate the observed (detector) time to real time in the molecular frame. A number of points must be considered in this regard: 1. Figure 8 shows the TOFMS signals as a function of time T as detected by the microchannel plate mass detector; 2. T is an implicit function of the fragmentation (real) time (t) of the parent clusters; 3. all signals are convolved with the instrument response function, as given by the toluene bare molecule signal; and 4. the mapping between t and T is a function of instrument parameters and the respective masses of the parent and fragment clusters, and thus different signal widths for different fragment clusters arising from a given parent do not necessarily imply different kinetics for each fragment.

To determine the lifetime of the immediate parent or precursor of $(\text{H}_2\text{O})_3\text{H}^+$ and to determine whether or not the fragments $(\text{H}_2\text{O})_3\text{H}^+$ and $\text{toluene}^+(\text{H}_2\text{O})_2$ have a common immediate parent before their formation, the time mapping for different ions ($t \leftrightarrow T$) must be found. This mapping is accomplished under the following assumptions: 1. the ion is formed at time zero at a single point within the ion extraction region; 2. parent clusters and their fragments have no initial velocity along the direction of the flight tube; and 3. the ions

are only directed by the applied electric field, not the presence of other ions. The resulting formulas are listed in Table III. Also presented is a flight time calculation for fragmentation occurring in the acceleration region. Evidently several factors which may potentially contribute to the observed signal (flight time) width have been ignored by these assumptions. The most significant one is probably the kinetic energy release associated with the various fragmentation channels. This initial fragment kinetic energy contribution to the ion flight time and its spread will be estimated in the ensuing discussion. All other contributions to the flight distribution for a given ion should effect all ions equally and thus may be included in the instrument response function (i.e., the observed width of the toluene⁺ signal).

Employing these two expressions with the experimental parameters given in Table III, one readily determines that the observed signal is generated only by cluster parent ion fragmentation in the ion extraction region. Since the electric field is so large in the acceleration region and the clusters spend so little time in this portion of the mass spectrometer, fragmentation in this region only contributes to the broad (unobserved) background signal extending from the fragment mass channel to the parent cluster (toluene(H₂O)₃) mass channel. Therefore, the observed signal width for (H₂O)₃H⁺ in either one- or two-color TOFMS (ca. 500 ns) is not directly related to any lifetime: this width merely indicates that the lifetime of the immediate parent of (H₂O)₃H⁺ is long enough that this cluster reaches the edge of the ion extraction grid with sufficient concentration for (H₂O)₃H⁺ to be detected following its fragmentation.

In fitting the signals for (H₂O)₃H⁺ and toluene⁺(H₂O)₂ fragments of the parent toluene(H₂O)₃ clusters three constraints must be considered. First, only a small portion of the total fragment signal can be detected in a time interval at any given instant. Taking the limit of this signal ($\Delta[D]/\Delta T$), the detected signal is proportional to $\frac{d[D]}{dT}$ (T = detector time) and not the concentration of D. Second, ¹³C-toluene contributes equally to

the toluene(H_2O)_{2,3} signals but not to the (H_2O)₃ H^+ signal. Third, the observed "two-color" signal intensities of (H_2O)₃ H^+ and toluene⁺(H_2O)₂ have different actual one-color and two-color signal contributions and therefore only the one-color MRES data are chosen for fitting and analysis.

Consider the general reaction



in which P is the immediate precursor of the daughter fragments D, D'. Then

$$d[\text{D}]/dt = k[\text{P}] \quad (9)$$

and the fragment signal intensity as a function of time t would exponentially decay as the total concentration of P decays. (In the ensuing discussion we simplify the notion [D] and [P] to D and P, respectively.) The fitting process thus involves the following steps: 1. assume an exponential decay for P as a function of t, $\text{P} = \text{P}[t]$; 2. $\frac{dD}{dt} = k[\text{P}(t)]$; 3. find dD/dT by converting detector time T into real time t, such that

$$dD/dT = (dD/dt)(dt/dT) = k[\text{P}\{t(T)\}](dt/dT); \quad (10)$$

and 4. convolve dD/dT represented in T with the appropriate instrument response function.

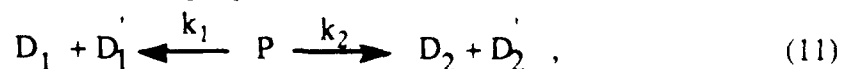
From the formulas given in Table III, one can readily determine that both $t(T)$ and dt/dT are required for the fitting and analysis procedure. A similar formula has been given for fragmentation in the ion extraction region only¹¹ (note some corrections, however), but dt/dT has not been employed. This derivative can be calculated from the expression for T given in Table III or can be approximated from $\Delta t/\Delta T$ away from the initial $t = 0$ point. Since the signal height is only known in a relative measure and is adjusted for a given scan the reaction constant k in eq. (10) does not directly enter into the analysis except as a scale factor.

Employing the equations given above and in Table III, the curve for the (H_2O)₃ H^+ signal can only be fit with two exponentials. The generation times are $\tau_1 = 60$ ns and $\tau_2 = 480$ ns: these decay times refer to the precursor decay times and suggest that

the $(\text{H}_2\text{O})_3\text{H}^+$ ion is generated by two different pathways. This fit is shown in Figure 10a in which the dashed curve is the experimental result and the solid curve is the bi-exponential fit with τ_1 and τ_2 . The same two lifetimes for the precursor give a poor fit to the experimental signal for toluene $(\text{H}_2\text{O})_2$ as displayed in Figure 10b: clearly the long lifetime ($\tau_2 \sim 480$ ns) is not appropriate for the decay of the immediate precursor to this daughter fragment ion. If only a single exponential with $\tau_1 = 60$ ns is fit to the experimental curve as shown in Figure 10c, a good reproduction of the experimental signal for the toluene $(\text{H}_2\text{O})_2$ fragment cluster obtains.

One can readily estimate the flight time spread due to initial kinetic energy of the fragment. Assuming that the fragment mass is 100 amu and that the initial kinetic energy of the fragment is 14 kcal/mol (~ 4900 cm $^{-1}$), the ion speed is 4.62×10^6 cm/s. A fragment ion of this speed moving away from the flight tube and mass detector would return to its original (creation) position in ~ 16 ns: this time is close to the instrument response function of 20 ns fwhm. The time of flight signal for toluene $^+(\text{H}_2\text{O})_2$ (see Figure 8) is somewhat wider than that of toluene. Thus the short lifetime τ_1 is stated as a maximum value: the actual generation time may be considerably less than the stated $\tau_1 < 60$ ns. The exact value of this fast component, however, does not affect any of the ensuing discussion of the cluster fragmentation kinetics and possible mechanisms.

In the following discussion we try to model the data with the simplest kinetic scheme consistent with above results. We begin by considering two simple mechanisms which cannot give rise to the bi-exponential decay times observed. The fitted curves presented in Figure 10 rule out a simple parallel kinetic scheme,

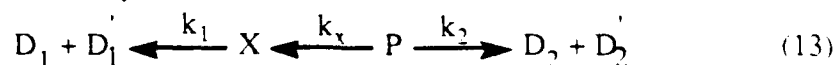


in which P is toluene $^+(\text{H}_2\text{O})_3$, D_1 is $(\text{H}_2\text{O})_3\text{H}^+$ and D_2 is toluene $^+(\text{H}_2\text{O})_2$. For parallel kinetics, one finds

$$dD_1/dt = k_1 P = (k_1/k_2) k_2 P = (k_1/k_2) dD_2/dt. \quad (12)$$

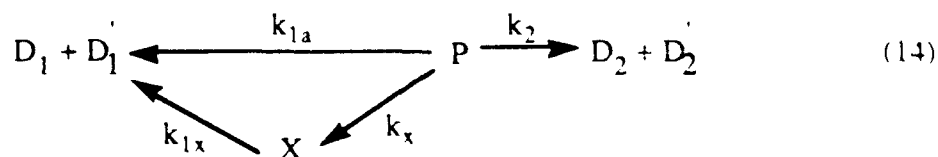
This would require that the two daughter fragment clusters have the same fitting parameters τ_1 and τ_2 : based on Figures 10a and 10b, this is clearly not the case. Eqs. (11) and (12) suggest single exponential kinetic behavior.

Since the immediate precursor of $(H_2O)_3H^+$ has both a fast and a slow decay and the immediate precursor of $\text{toluene}^+(H_2O)_2$ has only a fast decay, we can conclude that at least one precursor of $(H_2O)_3H^+$ cannot be P in the last equation. This precursor (represented by X) must be a daughter of P and have the same energy and stoichiometry as P. We then try,

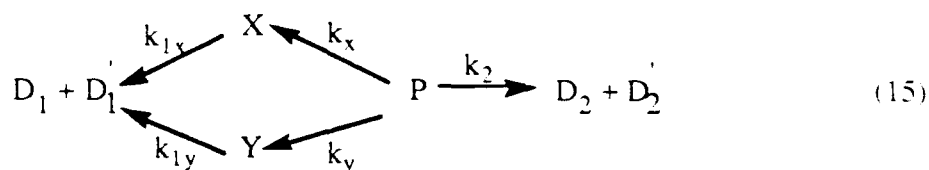


This kinetic equation yields dD_2/dt as a single exponential decay signal. dD_1/dt would rise and fall but still only with a single exponential behavior. In general, no matter how many products are generated from D_1 and no matter how many reaction pathways are involved, the number of decay components of dD_1/dt are unaltered in the above scheme. We must conclude the dD_1/dt ($d(H_2O)_3H^+/dt$) will have two decay components only if more than one species is detected simultaneously or if D_1 is generated from two different immediate precursors. Only the latter situation can obtain in our experiment.

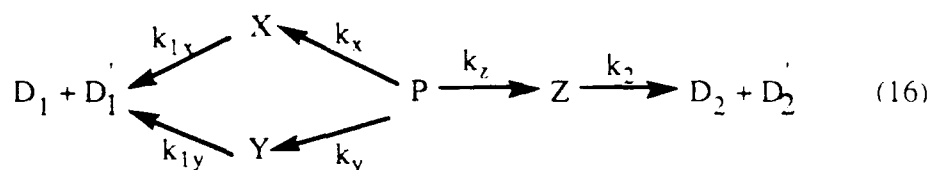
We can consider one of three possibilities for mechanisms that can represent the observed bi-exponential kinetics:



or



or



with $k_{1x} \ll k_{1y}$ or vice versa.

In these schemes X, Y could be two different states of the cluster created by IVR, two different proton transfer states (perhaps involving two different water molecules), or perhaps other combinations of states and cluster geometries. Since the short time constant is the same for D_1 and D_2 , eq. (14) and eq. (15) are similar kinetically but not necessarily mechanistically. The underlying conclusion from this presentation is that the overall decay of nascent toluene⁺(H₂O)₃ is not simple and may involve a number of distinct pathways and processes.

Without further detailed information concerning the structure, binding energy, and vibrational levels of the toluene⁺(H₂O)_{2,3} and (H₂O)₃H⁺ clusters, we cannot analyze these mechanisms further. We note, however, that a simple (classical) RRKM calculation of the form

$$k \propto c \left(\frac{E - E_0}{E} \right)^{S-1} h\nu$$

with E = total energy of cluster, E_0 = binding energy of the cluster, $c = 3 \times 10^{10}$ cm/s, $h\nu = 100$ cm $^{-1}$, $S = 18$, and $(E - E_0)/E \sim 0.75$ to 0.45 yields $\tau \sim 40$ ps to 300 ns. This range is reasonable in both time and energy balance for the overall reaction (Eq. 7) dynamics observed.

In larger clusters (toluene $^+(H_2O)_{3+m}$, $m = 1, 2, 3, \dots$) the energy balance is probably such that the proton transferred clusters containing the benzyl radical fragment much more rapidly. Only for the toluene $(H_2O)_3$ cluster is the gas phase basicity, benzyl radical solvation energy, and benzyl radical/ $(H_2O)_3H^+$ binding energy such that the reaction kinetics can be resolved with a ~ 20 ns fwhm instrumental response function.

These dynamics (i.e., fragment cluster generation times) are not observed for larger clusters such as toluene $^+(H_2O)_{4,5,6}$ for which enhanced cluster ion binding energies and enhanced basicities of the large water clusters yield a more highly vibrationally excited nascent state.

V. CONCLUSIONS

These studies of the ion chemistry in the toluene/water system have generated a number of conclusions. A summary of the reactions found, spectra assigned, and energy thresholds for the different dynamical behavior observed can be found in Tables I and II and Scheme I.

The general conclusions of this work can be stated as follows:

1. Toluene/water cluster ions undergo extensive fragmentation following one-color ($I \leftarrow S_1 \leftarrow S_0$) ionization. The favored fragmentation pathway for toluene $(H_2O)_n$, $n \leq 4$, is loss of a water molecule. At one-color excess energies (Table II), generation of toluene $(H_2O)_{n-1}$ by loss of a water molecule accounts for over 50% of the signal. The favored fragmentation pathway for toluene $(H_2O)_n$, $n \geq 5$ is the generation of $(H_2O)_nH^+$.
2. The number of toluene/water cluster geometries is quite small. Most clusters display a single spectroscopic origin and thus a single conformation for $n = 1, \dots$
6. The water molecules also seem to aggregate together (hydrogen bond) on one side of

the toluene ring. Cluster structure is suggested to be arranged in solvent shells with three water molecules forming a first shell and the others lying in a second shell.

3. Toluene⁺(H₂O)_n cluster ions ($n \geq 3$) can generate a benzyl radical and H⁺(H₂O)_{3+m} ($m = 0, 1, 2, \dots, n-3$) hydrated proton cluster ions. H⁺(H₂O)_n and the benzyl radical are the most probable fragmentation products.

4. The only observed intermediate state is S₁; T_n or S₀ are not involved in these processes.

5. Cluster ion fragmentation is so prevalent in aromatic/polar solvent clusters because stable products (e.g., benzyl radical, solvated protons, etc.) are generated and because cluster ion geometry is different from neutral cluster geometry. Polar solvents have large gas phase basicities ((H₂O)₃H⁺, . . .) and the Franck-Condon factor for the I ← S₁ transition is not large for Δv = 0 vibrational excitation. The ion cluster is thus created in a highly excited vibrational state for (most likely) both the van der Waals intermolecular modes and the toluene intramolecular modes.

6. Cluster reaction dynamics for toluene⁺(H₂O)₃ can be characterized. The reaction fragment (H₂O)₃H⁺ is generated through two separate pathways with generation times $\tau_1 < 60$ ns and $\tau_2 = 480$ ns. The reaction fragment toluene⁺(H₂O)₂ is generated with a single time constant $\tau_1 < 60$. Fragmentation dynamics of other clusters are too fast to measure within our instrument response function of ca. 20 ns fwhm.

Acknowledgement -

We wish to thank Professor D. F. Kelley for extensive and informative discussions concerning the kinetics of the observed processes.

REFERENCES

1.
 - a. R. Nowak, J. A. Menapace, and E. R. Bernstein, J. Chem. Phys. **89**, 1309 (1988).
 - b. Mark Schauer, K. Law and E. R. Bernstein, J. Chem. Phys. **82**, 726 (1985) and Mark, Schauer, K. Law and E. R. Bernstein, J. Chem. Phys. **82**, 736 (1985).
 - c. K. S. Law and E. R. Bernstein, J. Chem. Phys. **82**, 2856 (1985).
 - d. J. Wanna, and E. R. Bernstein, J. Chem. Phys. **84**, 927 (1986).
 - e. J. Wanna, J. A. Menapace and E. R. Bernstein, J. Chem. Phys. **85**, 1795 (1986).
 - f. M. R. Nimlos, D. F. Kelley and E. R. Bernstein, J. Phys. Chem. **93**, 643 (1989).
2.
 - a. A. Amiray U. Even and J. Jortner, J. Chem. Phys. **75**, 2489 (1981).
 - b. D. F. Kelley and E. R. Bernstein, J. Phys. Chem. **90**, 5164 (1986).
 - c. M. R. Nimlos, M. A. Young, E. R. Bernstein and D. F. Kelley, J. Chem Phys. **91**, 5268 (1989).
 - d. M. Hineman, D. F. Kelley, E. R. Bernstein, J. Chem. Phys., to be published.
3. S. K. Kim, S. Li, and E. R. Bernstein, J. Chem. Phys. **95**, 3119 (1991).
4. S.K. Kim, S. C. Hsu, S. Li and E.R. Bernstein, J. Chem. Phys. **95**, 3290 (1991).
5. S. Li and E. R. Bernstein, unpublished results.
6.
 - a. B. Brutschy, J. Phys. Chem. **94**, 8637 (1990).
 - b. B. Brutschy, C. Janes, and J. Eggert, Ber. Bunsenges. Phys. Chem. **92**, 74 (1988).
7.
 - a. A. J. Gotch, A. W. Garrett, D. L. Severance, and T. S. Zwier, Chem. Phys. Lett. **178**, 121 (1991).

- b. A. J. Gotch and T. S. Zwier, J. Chem. Phys., submitted.
- c. A. W. Garrett and T. S. Zwier, J. Chem. Pys., submitted.
- 8. S. Li and E. R. Bernstein, J. Chem. Phys. 0000, (1992) - following paper.
- 9. E. R. Bernstein, K. Law, and M. Schauer, J. Chem. Phys. **80**, 207 (1984).
- 10. a. K. S. Law and E. R. Bernstein, J. Chem. Phys. **82**, 2856 (1985).
- b. M. Schauer, K. S. Law, and E. R. Bernstein, J. Chem. Phys. **81**, 49 (1984).
- c. E. R. Bernstein, K. S. Law, and M. Schauer, J. Chem. Phys. **80**, 634 (1984).
- 11. J. L. Durant, D. M. Rider, S. L. Anderson, F. D. Proch, and R. N. Zare, J. Chem. Phys. **80**, 1817 (1984).

Table I. Identification of labeled transitions (in cm^{-1}).

	Transition Energy	Appearance in Mass Channels	Assignment
t	37,536	1C and 2C toluene	Toluene (internal methyl rotor)
-----	37,504 37,565 37,582 37,608	1C toluene; 2C T(W)_1	T(W)_1
p	37,579	1C and 2C T(W)_1 ;	Vibration, T(W)_2
q	37,531	2C T(W)_2	
a	37,606	1C and 2C T(W)_1 , T(W)_2 and $(\text{W})_3\text{H}^+$; 2C T(W)_3	Origin, T(W)_3
b	37,591	1C and 2C T(W)_3 , $(\text{W})_3\text{H}^+$ and $(\text{W})_4\text{H}^+$; 2C T(W)_4	Origin, T(W)_4
c	37,581	1C and 2C T(W)_3 , T(W)_4 , $(\text{W})_4\text{H}^+$ and $(\text{W})_5\text{H}^+$; 2C T(W)_5	Origins(?) T(W)_5
d	37,576		
e	37,567	1C and 2C T(W)_4 , $(\text{W})_5\text{H}^+$ and $(\text{W})_6\text{H}^+$; 2C T(W)_5	Origin, T(W)_6 or T(W)_7

Table II. Apparent ionization energy of toluene(H_2O)_n ($\text{T}(\text{H}_2\text{O})_n$) in cm^{-1} as detected by the appearance of different observed fragment signals. The numbers in parenthesis are the excess energies associated with the one-color ionization for each parent species and fragment.

Parent Cluster	T (n = 0)	$\text{T}(\text{H}_2\text{O})_1$ (n = 1)	$\text{T}(\text{H}_2\text{O})_2$ (n = 2)	$\text{T}(\text{H}_2\text{O})_3$ (n = 3)	$\text{T}(\text{H}_2\text{O})_4$ (n = 4)
Observed in Mass Channel					
$\text{T}(\text{H}_2\text{O})_n$	71090 (3870)	71070 (3950)	70640 (4420)	70075 (5140)	68940 (6240)
$\text{T}(\text{H}_2\text{O})_{n-1}$			71660 (3400)	71855 (3360)	70270 (4910)
$(\text{H}_2\text{O})_n\text{H}^+$				70940 (4280)	70060 (5120)

Table III. Time mapping between T as detected by the MCP detector and the real fragment time t after ionization.

Fragmentation in the extraction region (3.988kV to 3.655kV):

$$T = \sqrt{\frac{2}{e}} \left\{ \left(\frac{S_f M_p}{E_1} \right)^{1/2} + \sqrt{M_f} \left[\left(\frac{S_f C + S_1}{E_1} \right)^{1/2} - \left(\frac{S_f M_f}{E_1 M_p} \right)^{1/2} + \left(\frac{E_1}{E_2^2} (S_f C + S_1) + \frac{S_2}{E_2} \right)^{1/2} - \left(\frac{E_1 (S_f C + S_1)}{E_2^2} \right)^{1/2} + \frac{S_3}{2} \right] \right\}$$

$$(E_1 (S_f C + S_1) + E_2 S_2)^{-1/2} \left\{ \right\}$$

$$t = \left(\frac{2 S_f M_p}{E_1 e} \right)^{1/2}$$

Fragmentation in the acceleration region (3.655kV to 0.0kV):

$$T = \sqrt{\frac{2}{e}} \left\{ \sqrt{M_p} \left[\left(\frac{S_1}{E_1} \right)^{1/2} + \left(\frac{S_1 E_1}{E_2^2} + \frac{S_f - S_1}{E_2} \right)^{1/2} - \left(\frac{S_1 E_1}{E_2^2} \right)^{1/2} \right] + \sqrt{M_f} \left[\left(\frac{S_1 E_1 M_f}{E_2^2 M_p} + \frac{C (S_f - S_1)}{E_2} + S_2 \right)^{1/2} - \left(\frac{M_f}{E_2 M_p} \right)^{1/2} \right] \right\}$$

$$\left(\frac{S_1 E_1}{E_2} + S_f - S_1 \right)^{1/2} + \frac{S_3}{2} \left(\frac{S_1 E_1 M_f}{M_p} + S_2 E_2 + C E_2 (S_f - S_1) \right)^{-1/2} \left\{ \right\}$$

$$t = \sqrt{\frac{2 M_p}{e}} \left[\left(\frac{S_1}{E_1} \right)^{1/2} + \left(\frac{S_1 E_1}{E_2^2} + \frac{S_f - S_1}{E_2} \right)^{1/2} - \left(\frac{S_1 E_1}{E_2^2} \right)^{1/2} \right]$$

The first derivative evaluated at t = 0:

$$\frac{dT}{dt} \Big|_{t=0} = -C$$

Footnotes for Table III

Definition of Symbols used.

T = total flight time or the detected time,

t = fragmentation time,

S_0 = 12mm, distance between the bottom and the middle grids (3.988kV to 3.655kV),

S_1 = 7mm, distance between the ionization position and the middle grid,

S_f = distance between the ionization and the fragmentation positions,

S_2 = 12mm, distance between the middle and the top grids,

S_3 = 1480mm, distance between the top grid and the MCP detector,

M_p = 146amu, parent ion mass,

M_f = 55 or 128 amu, fragment ion mass,

E_1 = (3988V - 3655V)/ S_0 , electric field in the extraction region,

E_2 = 3655V/ S_2 , electric field in the acceleration region,

$C = M_f/M_p - 1$

Scheme I

Observed Fragmentations

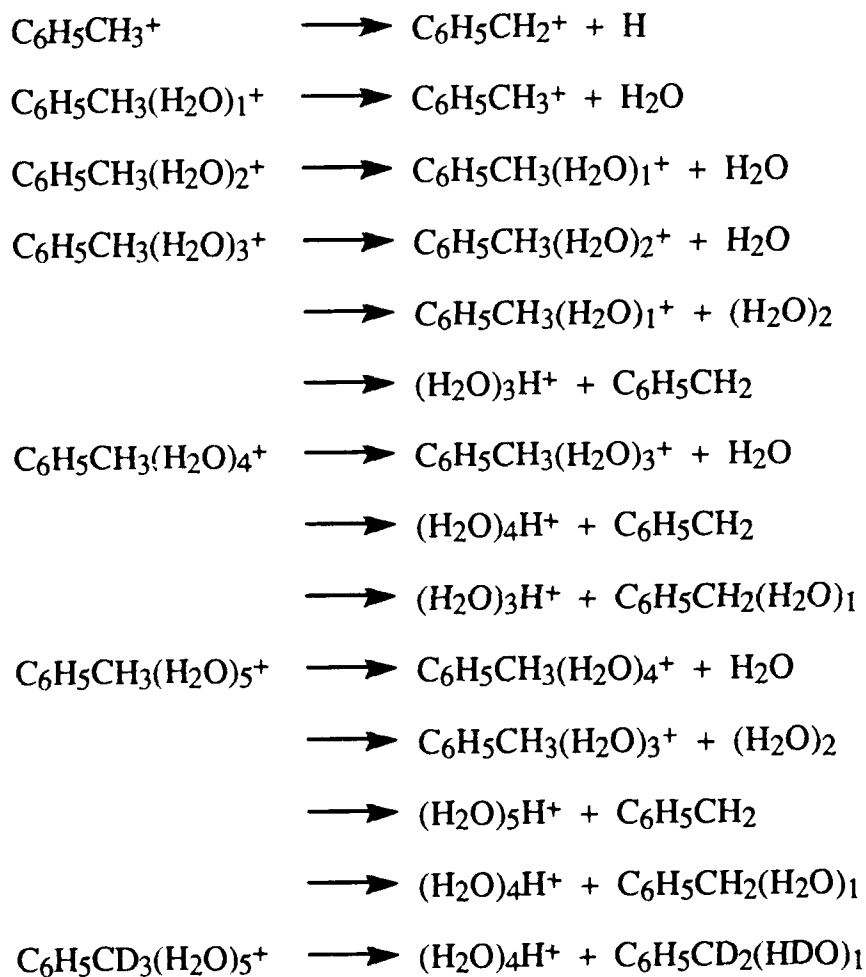


FIGURE CAPTIONS

- Figure 1: One-color mass resolved excitation spectra of toluene/water clusters observed in the toluene(H_2O) $_{n-1}$ mass channels. a: toluene(H_2O) $_1$, b: toluene(H_2O) $_2$, c: toluene(H_2O) $_3$, and d: toluene(H_2O) $_4$. Features labeled are discussed in the text. The mass channel designations in the figure (TW_m) refer to the detection channels not the true parent cluster masses.
- Figure 2: One-color mass resolved excitation spectra of toluene/water clusters observed in (H_2O) $_x\text{H}^+$ mass channels. a: (H_2O) $_3\text{H}^+$, b: (H_2O) $_4\text{H}^+$, c: (H_2O) $_5\text{H}^+$, and d: (H_2O) $_6\text{H}^+$. Features are labeled as in Figure 1.
- Figure 3: One-color mass resolved excitation spectra of toluene-d $_3$ /water clusters observed in (H_2O) $_x\text{H(or D)}^+$ mass channels. a: (H_2O) $_3\text{D}^+$, b: (H_2O) $_4\text{H}^+$, and c: (H_2O) $_4\text{D}^+$. Features are labeled with primed letters to correspond to features found for toluene(H_2O) $_x$ clusters.
- Figure 4: Two-color mass resolved excitation spectra of toluene/water clusters observed in toluene(H_2O) $_x$ mass channels. Second photon energy is in parentheses. a: toluene(H_2O) $_1$, b: toluene(H_2O) $_2$, c: toluene(H_2O) $_3$, d: toluene(H_2O) $_4$, and e: toluene(H_2O) $_5$. Features are labeled as in Figure 1. The arrows in the top spectrum point to new features suggested to be due to toluene(H_2O) $_1$.
- Figure 5: Identification of parent transitions of toluene(H_2O) $_1$. a: the difference spectrum of two-color mass resolved excitation spectra of toluene/water clusters observed in toluene(H_2O) $_1$ (Figure 4a) and in toluene(H_2O) $_2$ (Figure 4b) mass channels. T_i are toluene transitions and O_i are toluene(H_2O) $_1$ transitions. b: one-color mass resolved excitation spectra of toluene/water clusters observed in the toluene mass channel, in which toluene(H_2O) $_1$ transitions can be identified.

Figure 6: Time-of-flight mass spectra (TOFMS) of toluene/water clusters. Excitation laser frequency is in resonance with transition **b**. a: one-color spectrum, b: two-color spectrum with ionization laser energy 34350 cm^{-1} , and c: the same as b but with reduced ionization laser intensity.

Figure 7: Pulsed-nozzle/excitation-laser timing effect on signal intensities. These data can be used to associate specific cluster masses with specific transitions. See text for discussion.

Figure 8: One-color (top) and two-color (bottom) time-of-flight mass spectra of toluene/water clusters. Except for the toluene bare molecule signal, excitation laser frequency is in resonance with transition **a**. a: cluster signal observed beginning with $(\text{H}_2\text{O})_3\text{H}^+$ mass channel, b: toluene signal observed in toluene mass channel, c: cluster signal observed in toluene $(\text{H}_2\text{O})_2$ mass channel, and d: cluster signal observed in parent toluene $(\text{H}_2\text{O})_3$ mass channel. Identical behavior is observed for the $(\text{H}_2\text{O})_3\text{D}$ and toluene- $\text{d}_3(\text{H}_2\text{O})_2$ mass channels with the toluene- $\text{d}_3(\text{H}_2\text{O})_3$ parent cluster feature **a'** accessed. Extra features observed in the two-color mass spectrum of $(\text{H}_2\text{O})_3\text{H}^+$ are due to fragmentation caused by multiphoton ion absorption. While only the one-color feature is analyzed in detail, both are found to have the identical decay time constants.

Figure 9: Ionization action curves. a: toluene, b: benzene(methane) $_1$, and c: toluene $(\text{H}_2\text{O})_2$.

Figure 10: Expanded one-color time-of-flight mass spectra of toluene/water clusters, in resonance with transition **a**. Dashed line is the experimental data in Figures 8a through 8c and the solid line is the calculated fit. a: cluster signal observed beginning with the $(\text{H}_2\text{O})_3\text{H}^+$ mass channel and fit to 480 and 60 ns generation times, b: cluster signal observed in toluene $(\text{H}_2\text{O})_2$ mass channel and fit to the same weight of 480 and 60 ns generation times, and c: cluster signal observed in the toluene $(\text{H}_2\text{O})_2$ mass channel and fit with 60 ns generation time only.

1-COLOR MRES

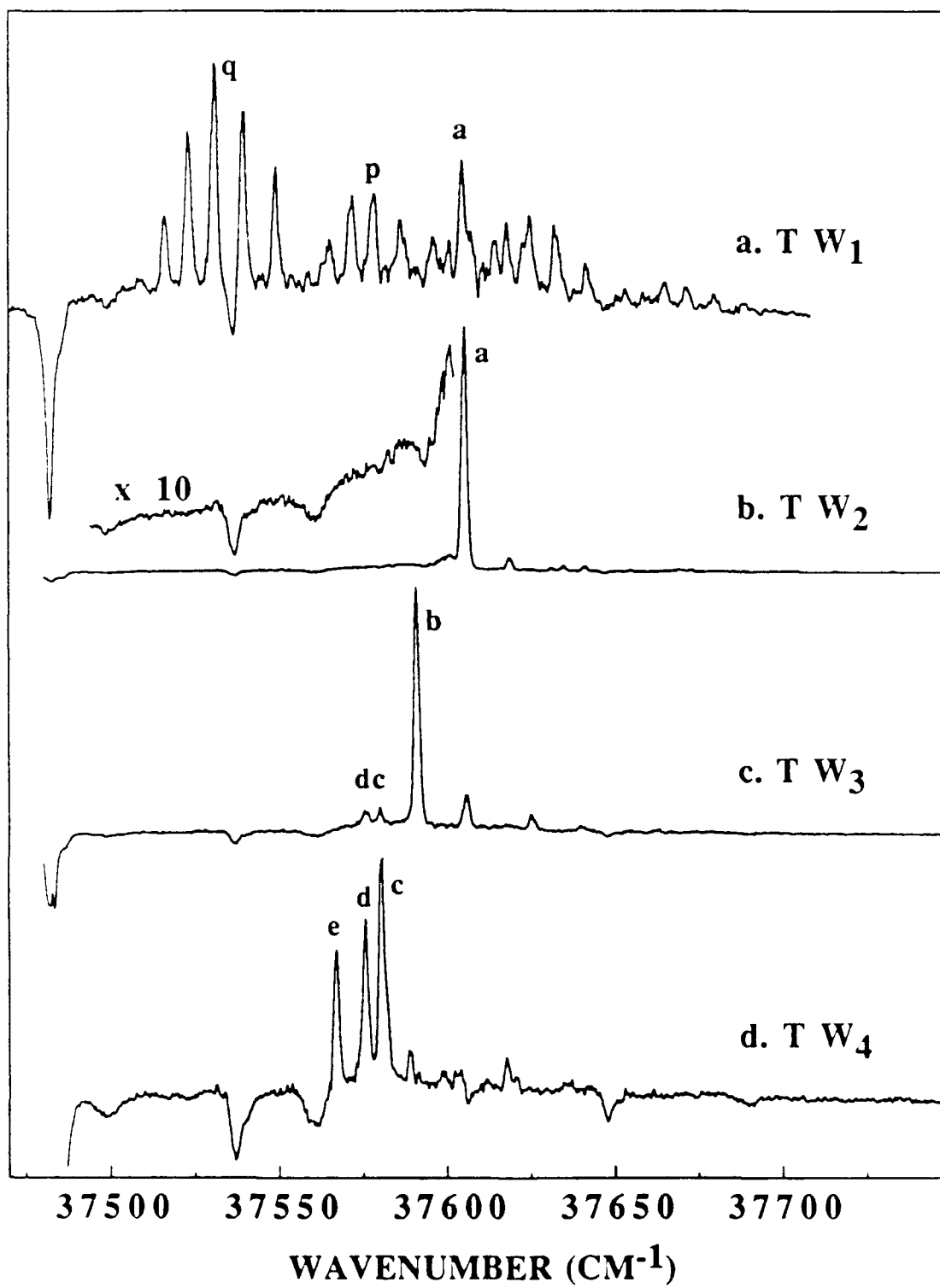


Figure 1

1-COLOR MRES

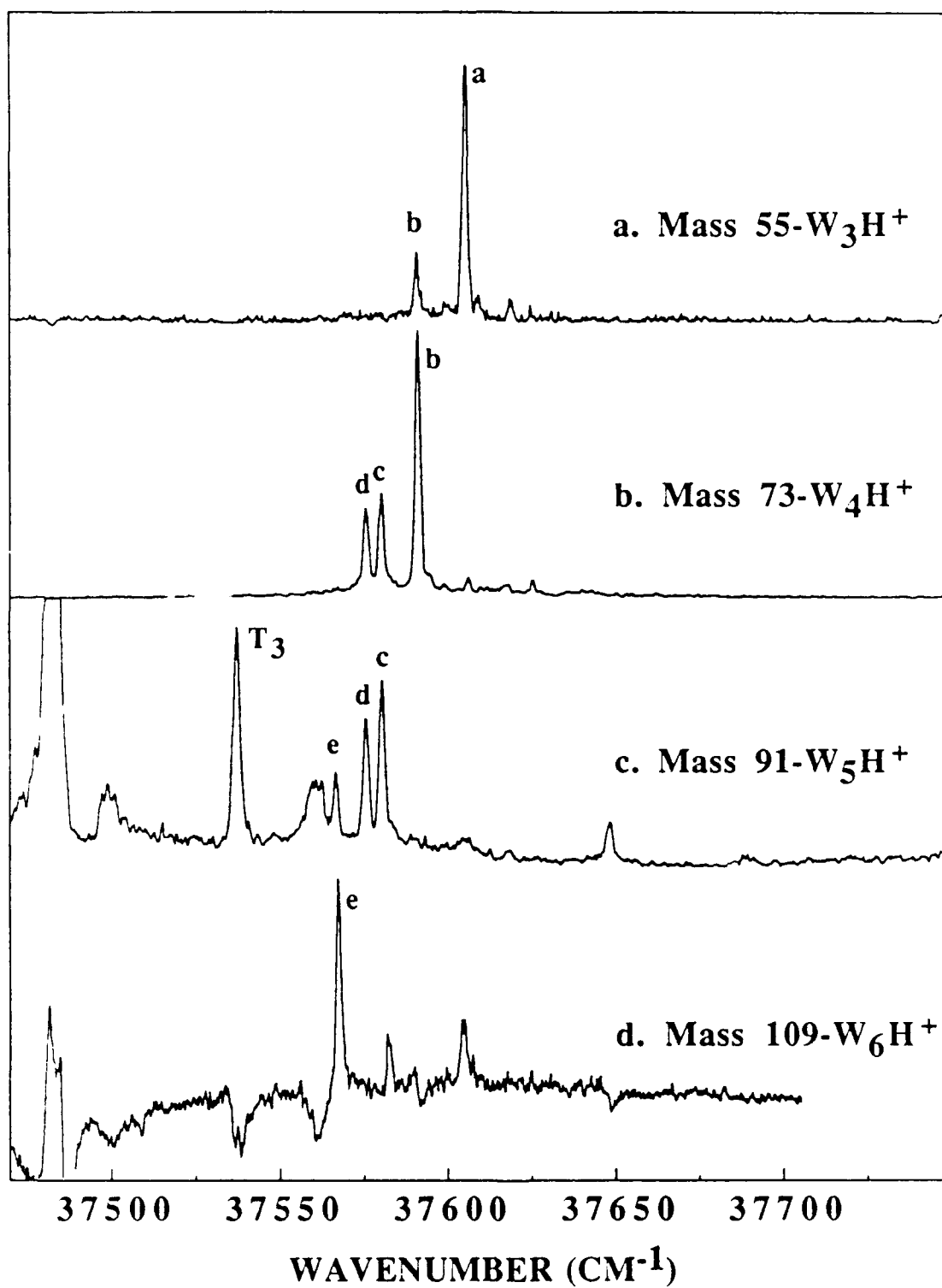


Figure 2

1-COLOR MRES: T-d₃

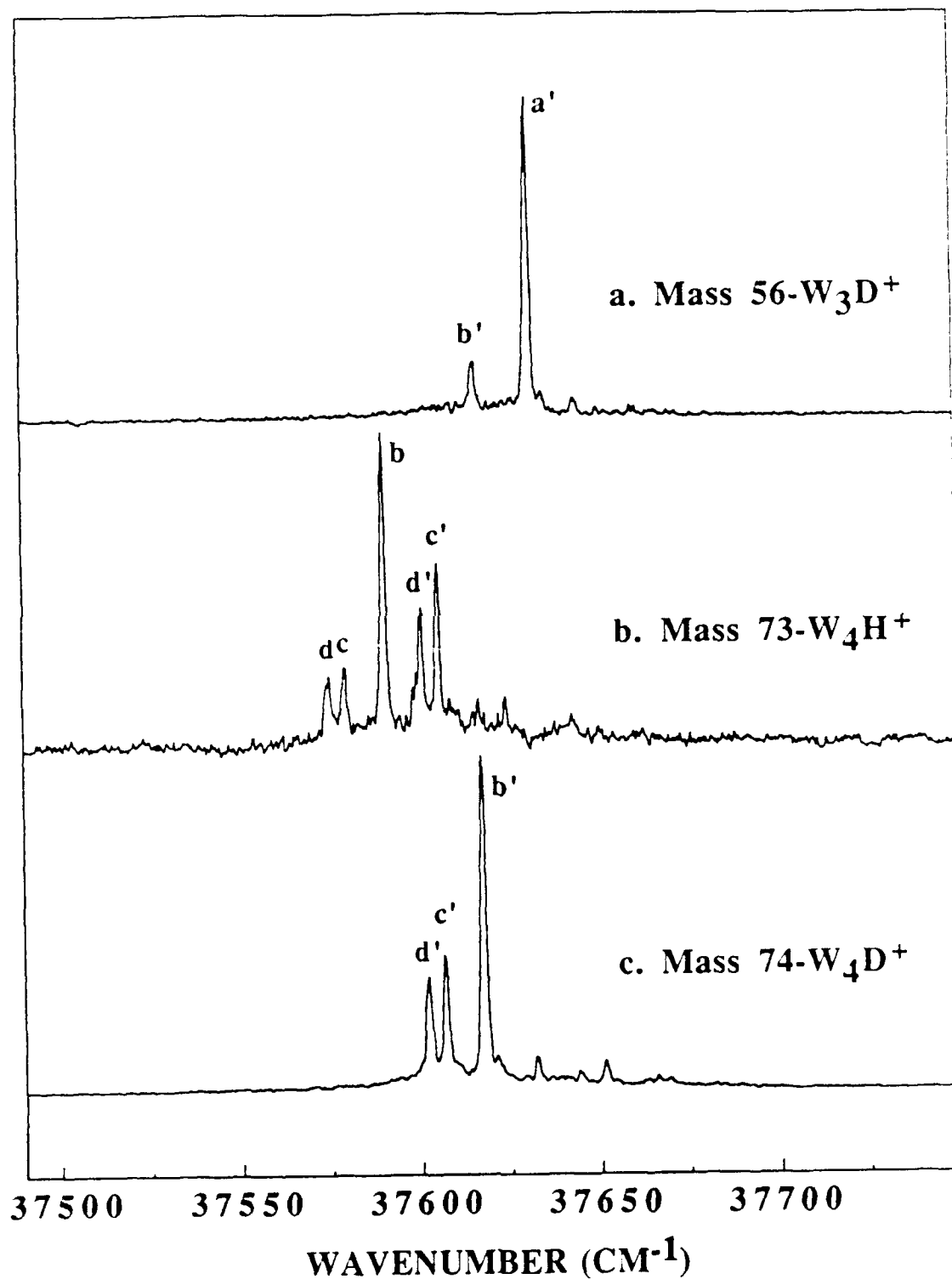


Figure 3

2-COLOR MRES

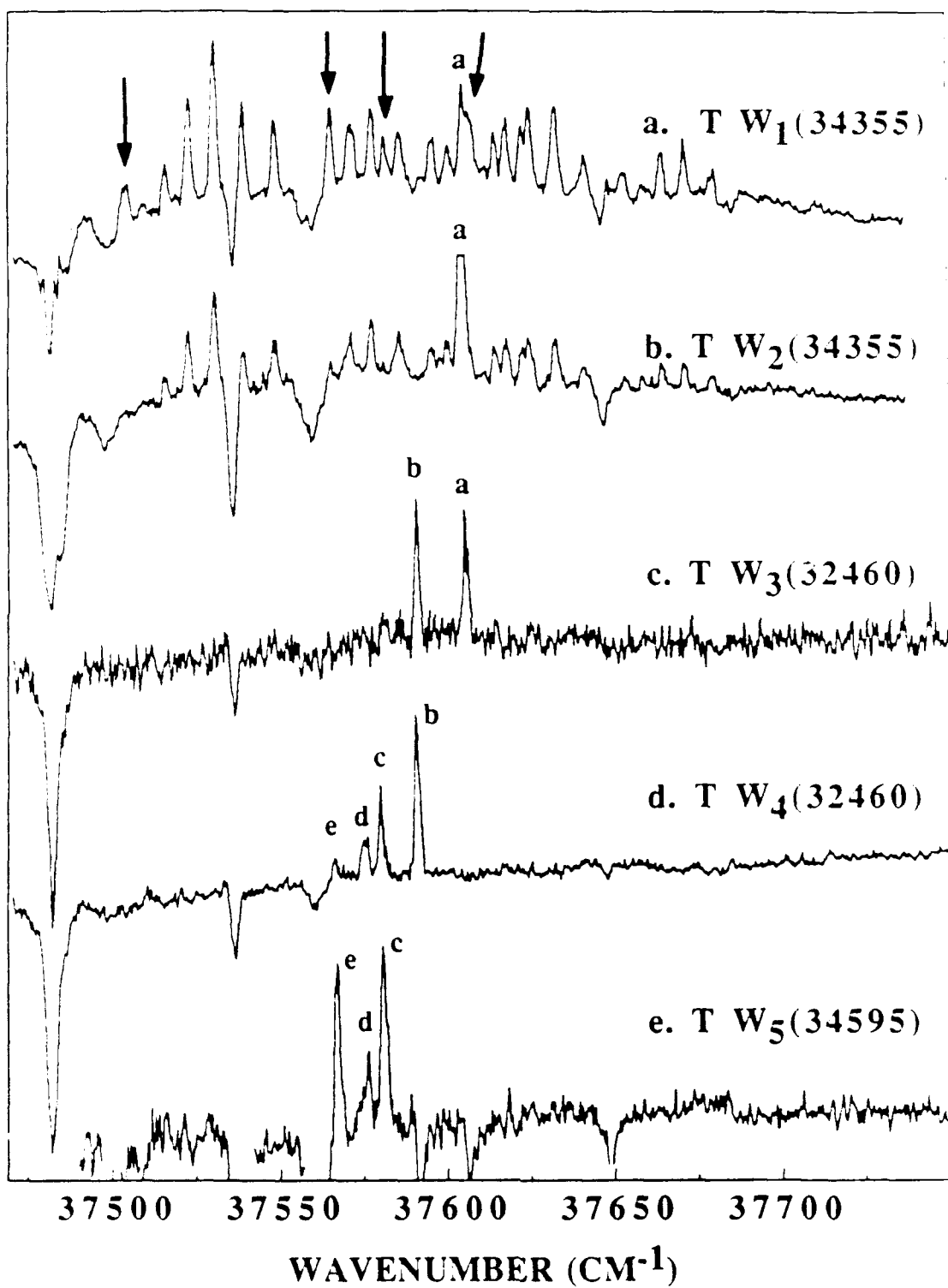


Figure 4

2-COLOR MRES: TOLUENE(H₂O)₁

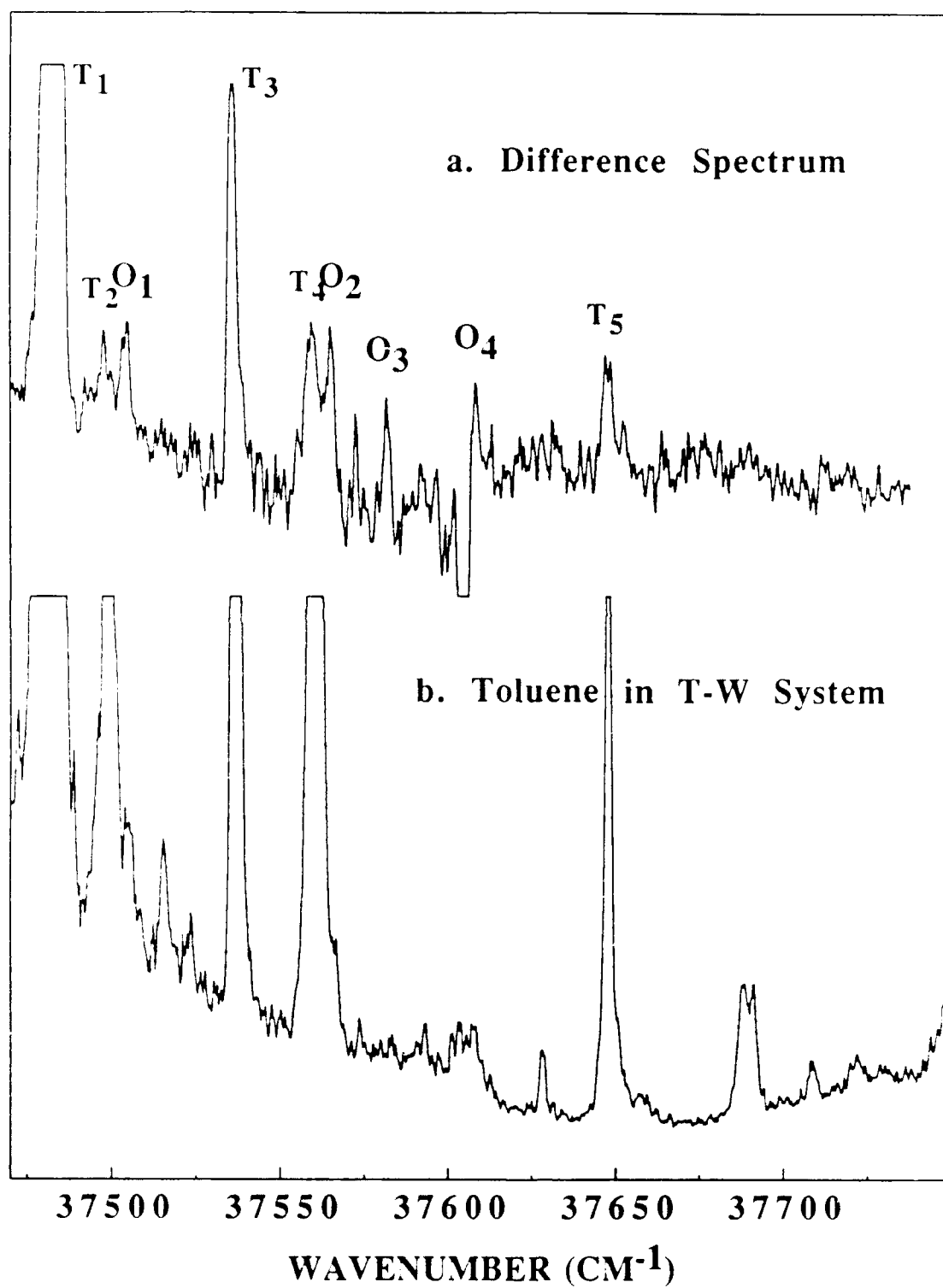


Figure 5

TOFMS: FEATURE b

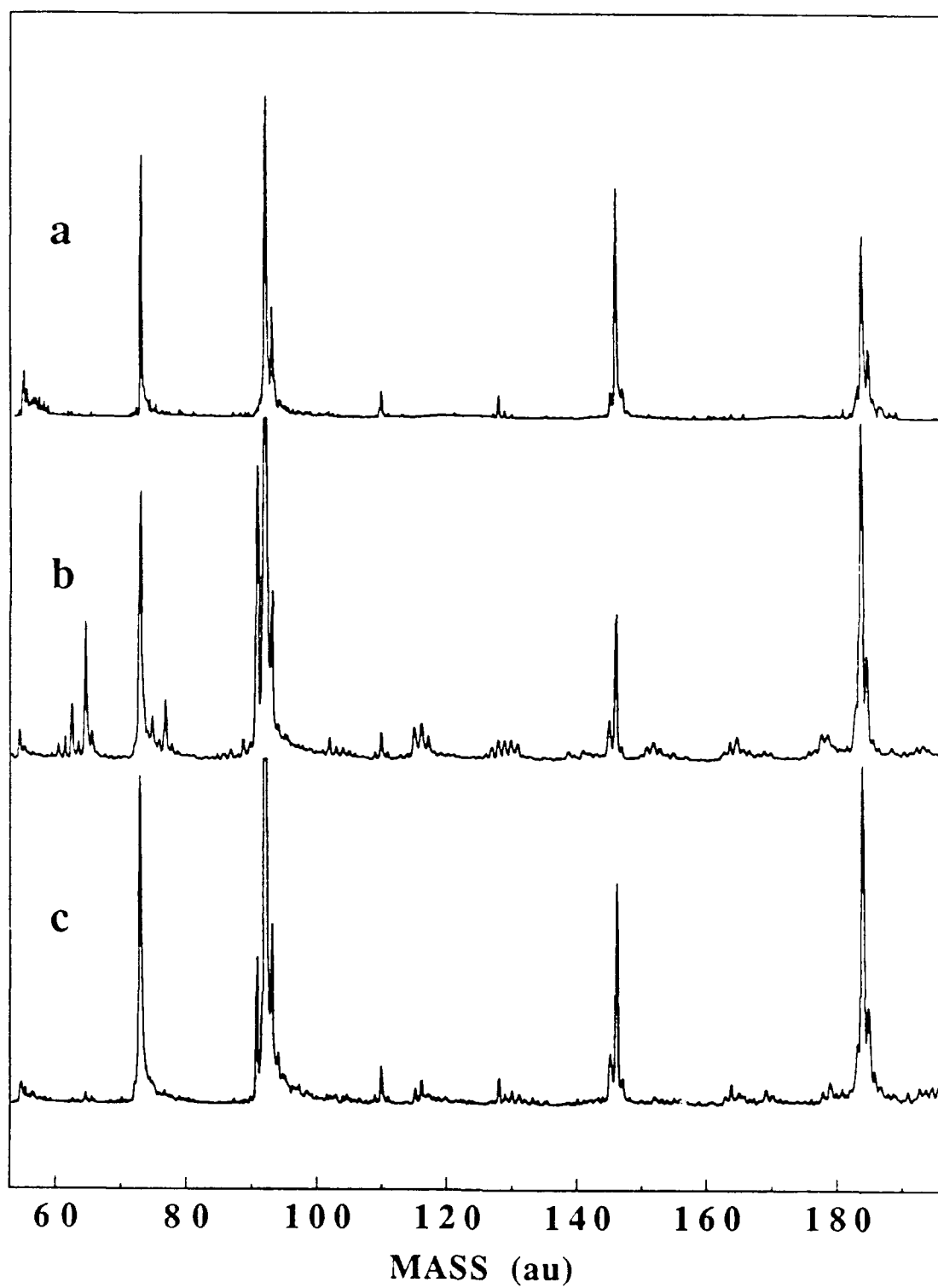


Figure 6

RELATIVE NOZZLE/LASER DELAY

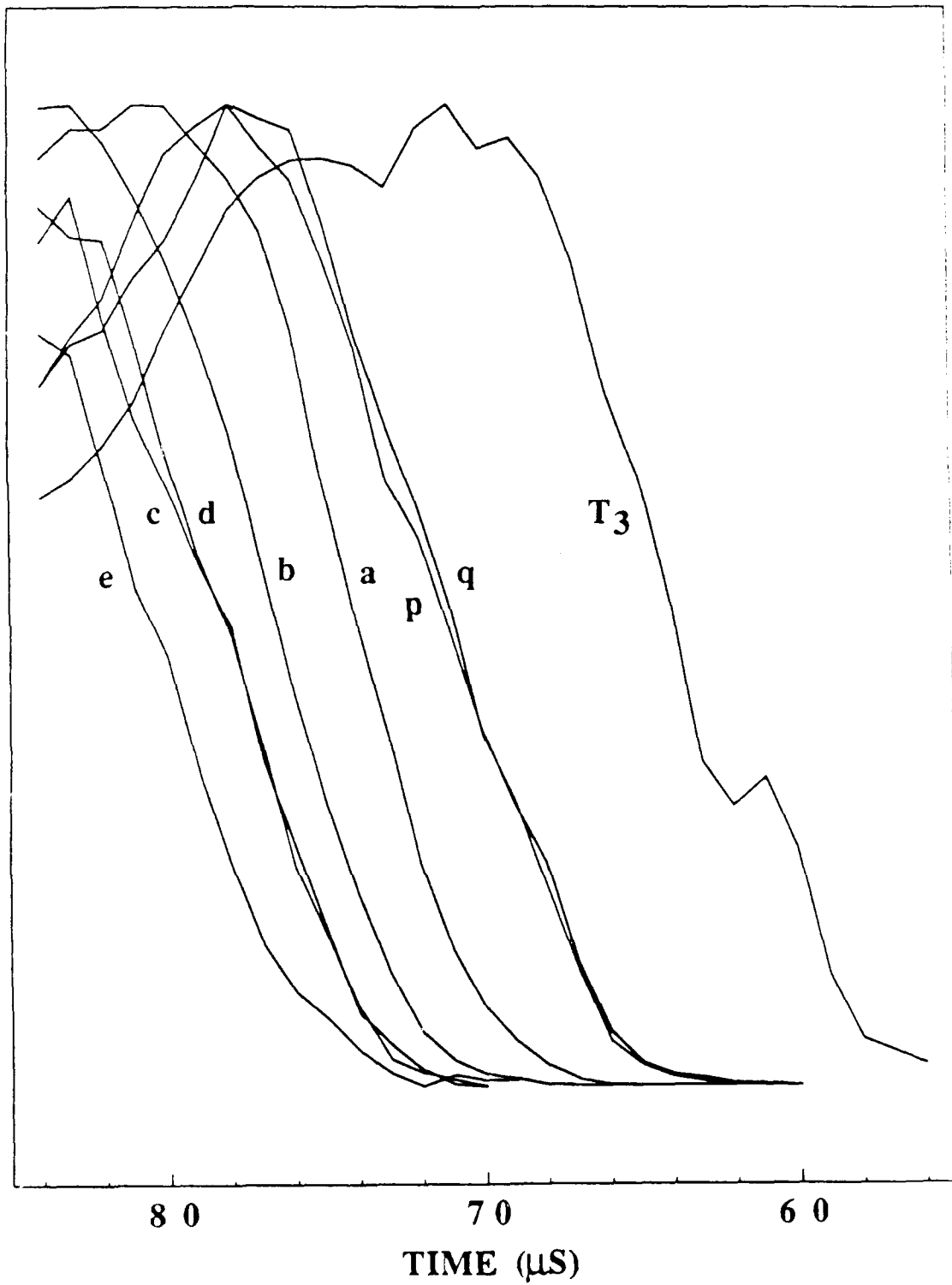


Figure 7

FRAGMENTATION TIME FOR TOLUENE(H_2O)₃

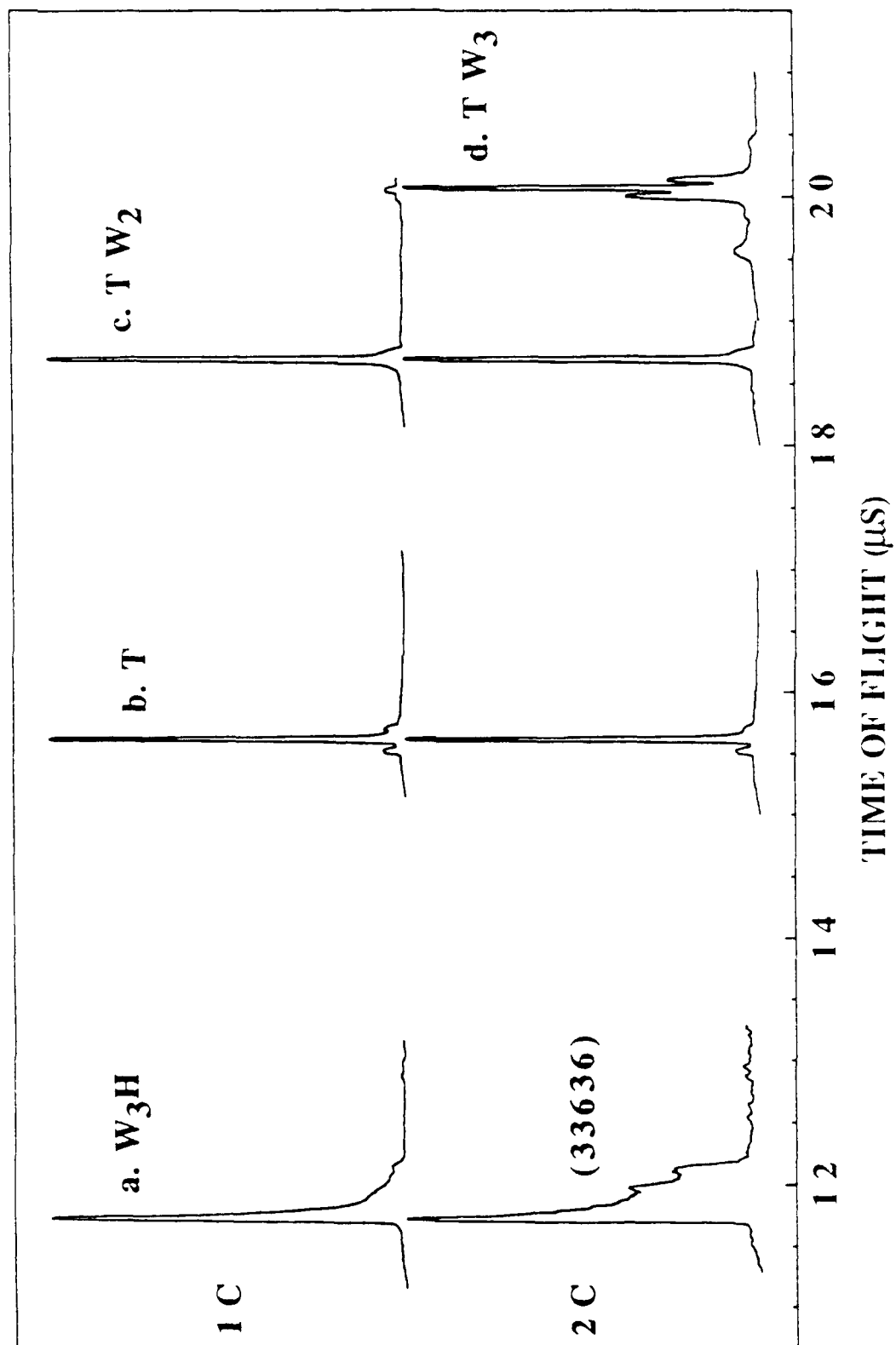


Figure 8

IONIZATION CURVES

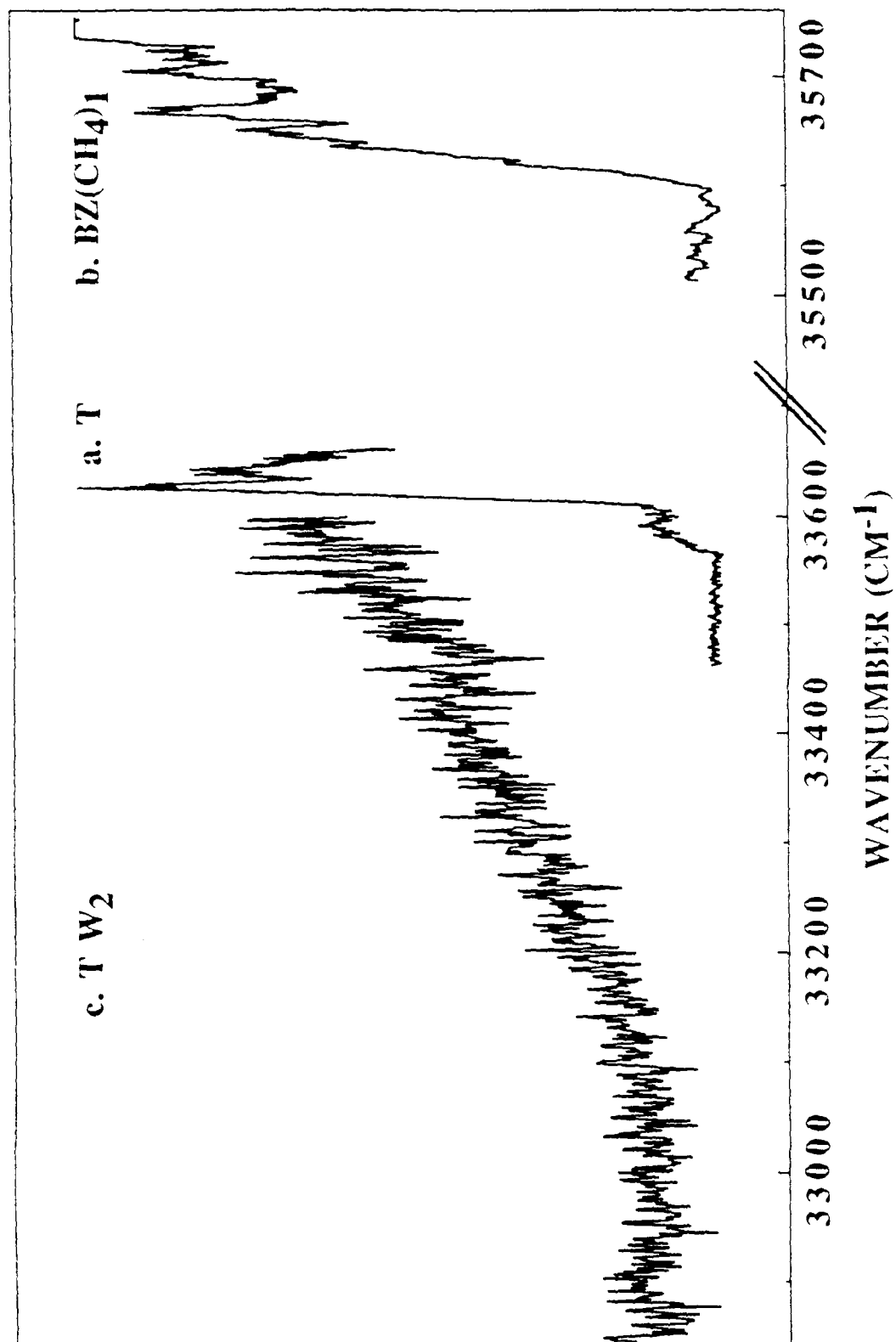


Figure 9

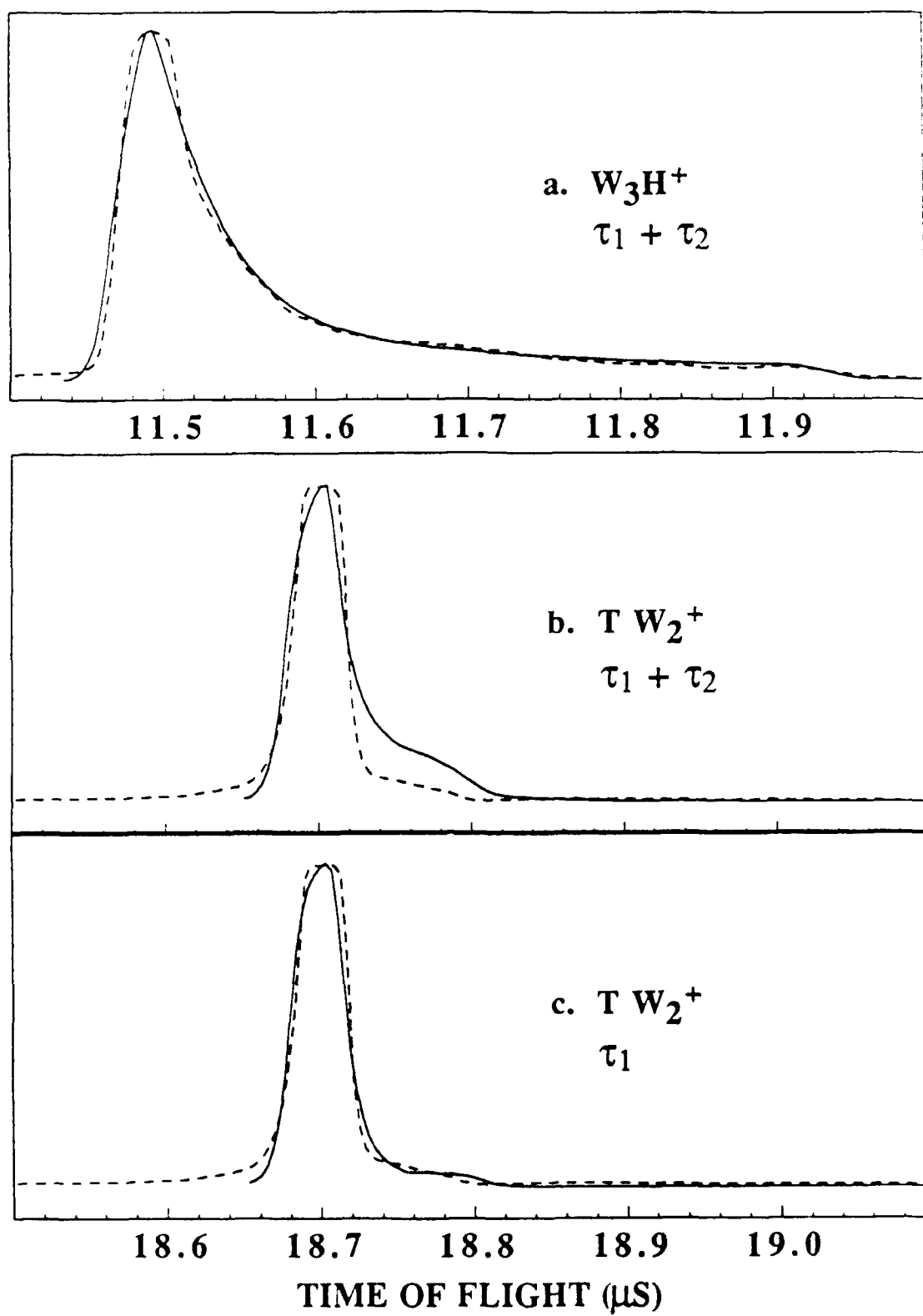


Figure 10